15

HIGHWAY RESEARCH BOARD

Bulletin 315

Bridge Dynamics and Deflections; And Fatigue in Welded Beams

National Academy of Sciences—
National Research Council

publication 961

HIGHWAY RESEARCH BOARD

Officers and Members of the Executive Committee

1962

OFFICERS

R. R. BARTELSMEYER, *Chairman* C. D. CURTISS, *First Vice Chairman*

WILBUR S. SMITH, *Second Vice Chairman*

FRED BURGGRAF, *Director* WILLIAM N. CAREY, JR., *Assistant Director*

Executive Committee

REX M. WHITTON, *Federal Highway Administrator, Bureau of Public Roads* (ex officio)

A. E. JOHNSON, *Executive Secretary, American Association of State Highway Officials* (ex officio)

LOUIS JORDAN, *Executive Secretary, Division of Engineering and Industrial Research, National Research Council* (ex officio)

PYKE JOHNSON, *Retired* (ex officio, Past Chairman 1960)

W. A. BUGGE, *Director of Highways, Washington Department of Highways* (ex officio, Past Chairman 1961)

R. R. BARTELSMEYER, *Chief Highway Engineer, Illinois Division of Highways*

E. W. BAUMAN, *Director, National Slag Association, Washington, D. C.*

DONALD S. BERRY, *Professor of Civil Engineering, Northwestern University*

MASON A. BUTCHER, *County Manager, Montgomery County, Md.*

J. DOUGLAS CARROLL, JR., *Director, Chicago Area Transportation Study*

C. D. CURTISS, *Special Assistant to the Executive Vice President, American Road Builders' Association*

HARMER E. DAVIS, *Director, Institute of Transportation and Traffic Engineering, University of California*

DUKE W. DUNBAR, *Attorney General of Colorado*

MICHAEL FERENCE, JR., *Executive Director, Scientific Laboratory, Ford Motor Company*

D. C. GREER, *State Highway Engineer, Texas State Highway Department*

JOHN T. HOWARD, *Head, Department of City and Regional Planning, Massachusetts Institute of Technology*

BURTON W. MARSH, *Director, Traffic Engineering and Safety Department, American Automobile Association*

OSCAR T. MARZKE, *Vice President, Fundamental Research, U. S. Steel Corporation*

J. B. MCMORRAN, *Superintendent of Public Works, New York State Department of Public Works*

CLIFFORD F. RASSWEILER, *Vice President for Research and Development, Johns-Manville Corporation*

GLENN C. RICHARDS, *Commissioner, Detroit Department of Public Works*

C. H. SCHOLER, *Applied Mechanics Department, Kansas State University*

WILBUR S. SMITH, *Wilbur Smith and Associates, New Haven, Conn.*

K. B. WOODS, *Head, School of Civil Engineering, and Director, Joint Highway Research Project, Purdue University*

Editorial Staff

FRED BURGGRAF
2101 Constitution Avenue

HERBERT P. ORLAND
Washington 25, D. C.

N.R.C. HIGHWAY RESEARCH BOARD

Bulletin 315

Bridge Dynamics and Deflections; And Fatigue in Welded Beams

Presented at the
40th ANNUAL MEETING
January 9-13, 1961

National Academy of Sciences —
National Research Council
Washington, D. C.
1962

$ 1.60

Department of Design

T. E. Shelburne, Chairman
Director of Research, Virginia Department of Highways
University of Virginia, Charlottesville

COMMITTEE ON BRIDGES
J. N. Clary, Bridge Engineer
Virginia Department of Highways, Richmond

Raymond Archibald, Kalispell, Montana
E. M. Cummings, Manager of Sales, Bethlehem Steel Company, Bethlehem, Pennsylvania
Frederick H. Dill, Assistant to Vice-President, Engineering, American Bridge Division, United States Steel Corporation, Pittsburgh, Pennsylvania
Arthur L. Elliott, Bridge Engineer, Planning , California Division of Highways, Sacramento
Eric L. Erickson, Chief, Bridge Division, Office of Engineering, Bureau of Public Roads, Washington, D. C.
R. S. Fountain, Bridge Engineer, Portland Cement Association, Chicago, Illinois
F. M. Fuller, Assistant Vice-President, Raymond International, Inc. New York, N. Y.
H. deR. Gibbons, The Union Metal Manufacturing Company, Canton, Ohio
John J. Hogan, Consulting Structural Engineer, Portland Cement Association, New York, N. Y.
W. T. Lankford, Applied Research Laboratory, United States Steel Corporation, Monroeville, Pennsylvania
Adrian Pauw, Professor of Civil Engineering, University of Missouri, Columbia
M. N. Quade, Consulting Engineer, Parsons, Brinckerhoff, Quade and Douglas, New York, N. Y.
William H. Rabe, Columbus, Ohio
C. P. Siess, Department of Civil Engineering, University of Illinois, Urbana
Charles B. Trueblood, Armco Drainage and Metal Products, Inc., Middletown, Ohio
George S. Vincent, Bureau of Public Roads, Washington, D. C.

Department of Materials and Construction

John H. Swanberg, Chief Engineer,
Minnesota Department of Highways,
St. Paul

GENERAL MATERIALS DIVISION

C. E. Minor, Chairman
Washington State Road Commission, Olympia
M. G. Spangler, Vice-Chairman
Iowa State University

COMMITTEE ON METALS AND WELDING

LaMotte Grover, Chairman
Air Reduction Sales Company, New York

Randle B. Alexander, Bridge Engineer, Texas Highway Department, Austin

Warren G. Alexander, Senior Civil Engineer (Design), New York State Department of Public Works, Albany

John L. Beaton, Supervising Highway Engineer, Materials and Research Department, California Division of Highways, Sacramento

Gordon Cape, Manager of Technical Research, Dominion Bridge Company, Ltd., Montreal, Canada

Frank Couch, Welding Engineer, Bethlehem Steel Company, Bethlehem, Pennsylvania

E. S. Elcock, Bridge Engineer, State Highway Commission of Kansas, Topeka

Eric L. Erickson, Chief, Bridge Division, Office of Engineering, Bureau of Public Roads, Washington, D. C.

G. O. Hoagland, Development Department, Aluminum Company of America, New Kensington, Pennsylvania

I. O. Jahlstrom, Bridge Engineer, Operations, California Division of Highways, Sacramento

Arthur W. Moon, Office of Deputy Chief Engineer, Structures, New York State Department of Public Works, Albany

Robert A. Norton, Bridge Engineer, Connecticut State Highway Department, Hartford

D. H. Overman, Columbus, Ohio

Contents

Dynamic Behavior of Simple-Span Highway Bridges

ROBERT K. WEN, Assistant Professor of Civil Engineering, Michigan State University, and A. S. VELETSOS, Professor of Civil Engineering, University of Illinois

● This paper presents the results of an analytical study on the dynamic behavior of simple-span highway bridges traversed by heavy vehicles. The factors that affect the dynamic response of such bridges are reviewed, and the influence of several of these are discussed. The factors considered include the speed of the vehicle, the spacing of the vehicle axles, the dynamic conditions of the bridge and the vehicle as the vehicle enters on the span, and the unevenness of the bridge surface. Most of these factors have been found in field tests to be responsible for major dynamic effects in highway bridges(1).

The approach used in this study consists in taking certain "representative" bridges and vehicles, and evaluating the effects of the parameters enumerated above by varying one parameter at a time. The bridges considered are of the I-beam type with span lengths in the range between 20 and 78 ft. This type of bridge consists of a series of steel girders and a reinforced concrete slab. With a few exceptions, the vehicle loading used corresponds to the heavy rear axles of a tractor-semitrailer combination with weights equal to those of the rear axles of an H20-S16 vehicle.

In the analysis, the bridge is idealized as a simply supported beam and the vehicle as a two-axle sprung load unit. Since the system is considered to have no width, the effects of the torsional oscillations of the bridge and the rolling of the vehicle about its longitudinal axis cannot be taken into account. The representation of the vehicle as a two-axle load is one of the distinguishing features of this study.

The idealized system is analyzed on the assumption that the instantaneous deflection configuration of the neutral axis of the beam is proportional to the corresponding static configuration produced by the weight of the vehicle and the weight of the bridge itself. In effect, this assumption reduces the beam to a system with a single degree of freedom and simplifies the analysis of the problem. The method has been programmed for the ILLIAC, the electronic digital computer of the University of Illinois. The results presented herein were obtained by application of this computer program.

Analytical studies of the dynamic response of highway bridges under moving vehicles have been reported in several publications. The effects of speed and of the initial vertical motion of the vehicle are discussed in Tung et al. (2) and Biggs et al. (3) by idealizing the vehicle as a single-axle load. The two-axle load used in the present study is obviously a more realistic representation of the vehicle. It enables one to take into account the effects of such variables as the spacing of the axles and the pitching motion of the vehicle. Field tests data (4) have given evidence of increased dynamic effects when the period of axle applications (i.e., the time between the passing of successive axles over a given point on the bridge) is synchronized with the fundamental natural period of vibration of the bridge.

The first analytical investigation of the dynamic effects produced by multiple-axle loads was published by Looney (5), who considered both two-axle and three-axle loads. Each axle load was represented either as a moving force of constant magnitude or as a smoothly running unsprung mass. The effect of vehicle suspension was not considered. Some exploratory studies of the influence of roadway unevenness have been reported by Scheffey (6) and Edgerton and Beecroft (7). In the present study, these parameters are studied in greater detail than in any of the previous publications.

METHOD OF ANALYSIS

System Considered

The idealized beam-load system used to represent the actual bridge-vehicle system is shown in Figure 1. It consists of a simply supported, linearly elastic beam spanning between two rigid supports on a horizontal line, and a two-axle load moving from left to right at a constant speed.

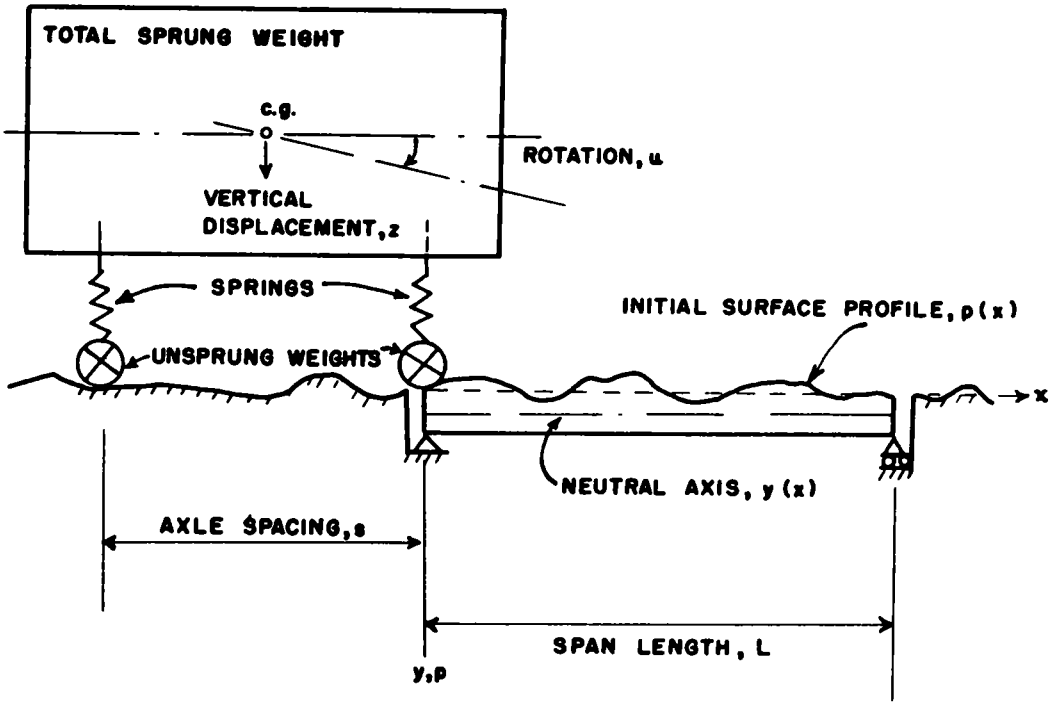

Figure 1. Idealized bridge-vehicle system.

Although the surface of the beam may be uneven, the beam itself is assumed to be of uniform mass and flexural rigidity per unit of length. In other words, the magnitude of the unevenness is assumed to be so small that its effect on the distribution of the mass and flexural rigidity of the beam along the span is negligible. This assumption is realistic because the height of the unevenness in actual bridges is usually small in comparison with the depth of the bridge. (In Figure 1 the magnitude of the unevenness is greatly exaggerated.)

The two-axle load consists of a rigid "sprung mass" connected to two "unsprung masses" through two linearly elastic springs. The unsprung mass is considered to be in direct contact with the roadway surface. The sprung mass represents the mass of the payload and chassis of the vehicle, and the unsprung masses represent the mass of the axles and tires. The springs simulate the flexibility of the suspension system and/or tires. It should be noted that no damping is considered in either the vehicle or the bridge model.

In the following discussion, the terms "beam" and "bridge" and the terms "load" and "vehicle" are used interchangeably.

Analysis of Idealized System

The beam is analyzed as a system with a single degree of freedom. This is done by specifying the shape of its deflection curve at any instant. Specifically, it is assumed that the instantaneous dynamic deflection configuration of the beam is proportional to that produced by the weight of the moving load and the weight of the beam itself applied statically. Throughout the time that the vehicle is on the span, the axles of the vehicle are considered to be in contact with the beam or the approach pavement. The analysis is based on the ordinary beam theory which neglects the effects of shearing deformation and rotary inertia.

With the above simplifications, the behavior of the bridge-vehicle system can be described in terms of three second-order linear differential equations with variable coefficients. The three unknown functions are the vertical displacement of the center of gravity of the sprung weight of the vehicle, z (see Figure 1), the angular displacement of the sprung weight, u, and a function f(t) relating the instantaneous dynamic deflection of the beam to the corresponding static deflection. These equations were solved by a step-by-step method of numerical integration. For each time interval, the displacements z and u and the function f(t) are first determined. Next, the instantaneous reactions between the unsprung masses and the beam surface, and the inertia forces due to the mass of the beam are evaluated. Finally, the bending moments in the beam are determined from the instantaneous loading on the beam in the same manner as for a static problem. For the details of the method of analysis, the reader is referred to Wen (8).

Problem Parameters

The parameters that affect the response of the idealized system considered here may conveniently be classified as "bridge parameters" and "vehicle parameters." The bridge parameters include the span length, total weight, and fundamental natural period of vibration of the bridge; the deviation, if any, of the bridge surface from a straight line through the end supports; and the initial dynamic condition of the bridge. The term "initial condition" is used to designate the dynamic displacement and the velocity of the bridge at the instant the vehicle enters the span. It is conceivable that these quantities may be different from zero, because when the vehicle enters the span the bridge may already be in a state of oscillation due to the previous passage of another vehicle.

The vehicle parameters include the speed and total weight of the vehicle, the distribution of the weight among its unsprung and sprung components, the spacing of the axles, the effective spring constant for axle, and the initial dynamic condition of the vehicle. It is possible that at the instant the vehicle enters the span, the sprung weight of the vehicle may have a bouncing or a pitching motion, or a combination of the two. This motion may be due to the unevenness of the approach pavement, or it may result from a discontinuity at the bridge entrance.

In the analysis, these variables are combined into the following dimensionless parameters:

The Speed Parameter. —Denoted by the symbol α, this parameter is defined by the equation

$$\alpha = \frac{vT_b}{2L} \tag{1}$$

in which v is the speed of the vehicle, T_b is the fundamental natural period of vibration of the bridge, and L is the span length (for symbols see Appendix).

For the type of highway bridge considered herein, the period T_b is for all practical purposes proportional to L. Hence, the parameter α is essentially a function of the vehicle speed only.

The Weight and Weight Distribution Parameters. —The weight parameter is defined as the ratio of the total weight of the vehicle to the total weight of the bridge. The weight distribution parameters include the ratio of the static reactions on the two

axles and the ratios of the unsprung weight for each axle to the total weight of the vehicle.

Frequency Parameters.—Associated with each axle j (j = 1 or 2), there is a frequency parameter defined as the ratio

$$\frac{(f_v)_j}{f_b} = \frac{\text{"Natural Frequency of } j^{th} \text{ Axle"}}{\text{Fundamental Natural Frequency of Bridge}}$$

The axle frequency, $(f_v)_j$, is defined by the equation

$$(f_v) = \frac{1}{2\pi}\sqrt{\frac{k_j}{M_j}} \tag{2}$$

in which k_j is the effective stiffness of the j^{th} axle, and M_j is the corresponding sprung mass. The sprung mass for an axle is the mass corresponding to the static reaction on the axle due to the sprung weight of the vehicle. It should be pointed out that only in special cases does the axle frequency $(f_v)_j$ represent the actual natural frequency of the vehicle in either the vertical mode or the pitching mode of vibration.

Rotary Inertia Parameter.—This parameter is a measure of the resistance of the sprung mass of the vehicle against pitching motion, and it is defined by the ratio

$$\frac{J}{\sum_{j=1}^{2} M_j a_j^2}$$

in which J is the polar moment of inertia of the sprung mass about its centroidal axis, M_j is the sprung mass for the j^{th} axle, as previously defined, and a_j is the horizontal distance between the j^{th} axle and the centroid of the sprung mass. The value of this parameter depends on the geometry of the sprung mass and the spacing of the axles. The expression in the denominator of this ratio represents the polar moment of inertia of the sprung mass when the masses M_j are concentrated at the axles. Thus, when this ratio is unity, the two-axle load can be thought of as two separate and independent single-axle loads, each consisting of a sprung and an unsprung mass.

Axle Spacing Parameter.—This parameter represents simply the ratio s/2L, where s is the spacing of the axles.

Initial Condition Parameters for Bridge.—The initial condition of the bridge may be defined by the dynamic deflection and the velocity of the structure at the instant the front axle of the vehicle enters the span. The expressions for these quantities are presented later.

Initial Condition Parameters for Vehicle.—The initial condition of the vehicle may be defined by the vertical and angular displacements and velocities of the sprung mass of the vehicle at the instant the front axle enters the span. The expressions for these quantities are also given later.

Initial Profile Parameters.—These parameters specify the shape of the bridge surface when the bridge is in a position of equilibrium under the influence of its own weight only. The number of parameters required depends on the degree of regularity of the initial profile. For example, if the profile can be represented by a mathematical expression, such as a sine function, one need specify only the amplitude and the length of the sinusoidal wave. At the other extreme, if the profile is quite irregular, one must specify its elevation at a large number of stations along the span. In this case, the number of parameters needed is equal to the number of stations used. Obviously, the latter technique may be used also for any profile representable by a simple mathematical function.

Computer Program

The method of analysis has been programmed for the ILLIAC, the high-speed digital computer of the University of Illinois. With the program developed, it is possible to consider any practical combination of the parameters enumerated in the preceding section. By an appropriate choice of the weight distribution parameters, it is also possible to consider the effects of a two-axle, totally sprung load, or of two unsprung point masses. It is also possible to consider the case of two independent one-axle loads, each consisting of a sprung and/or unsprung mass, as well as the case of a single one-axle load. These are simply "degenerated" cases of the more general two-axle load unit shown in Figure 1.

The program can handle a sinusoidal profile variation with a maximum of 33 half-sine waves along the span, and any other nonsystematic profile that can be prescribed by the values of the ordinates at 100 stations equally spaced along the span.

To use the program, one need only prepare a "parameter tape" on which are recorded the values of the parameters defining the problem to be solved. This tape is then read by the computer following a "master tape" that contains appropriate machine instructions for the analysis of the problem. The results computed include the dynamic deflection and the maximum static deflection at midspan, and the amplification factors for bending moment at midspan and at sections beneath the axles. The term "amplification factor" is defined as the ratio of the total dynamic effect at a section to the corresponding absolute maximum static effect at the same section. For example, the amplification factor for bending moment at a section beneath the rear axle of the vehicle represents the ratio of the instantaneous dynamic moment at that section to the corresponding absolute maximum static moment.

A complete solution, covering the period between the instant the front axle moves on the span and the instant the rear axle leaves the span, is obtained in about 3 min. This time can be halved if the computer is instructed to print out only the maximum values of the quantities referred to above.

SCOPE OF STUDY

Approach

The approach used in this investigation consists in considering specific bridges and vehicles and evaluating the dynamic behavior of these systems by varying each of the following parameters: (a) speed of the vehicle, (b) spacing of the axles, (c) initial condition of the bridge, (d) initial condition of the vehicle, and (e) unevenness of the bridge surface.

It is realized that the effects of these factors cannot actually be isolated because of the interrelations among their roles and influences. For example, when the effect of axle spacing is being considered, the influence of vehicle speed is inseparably involved. In this presentation, each factor will be treated separately, but mention will be made of any important interrelations that exist between the various parameters.

For each problem, the response of the bridge was evaluated for the time interval between the entry of the front axle on the span and the exit of the rear axle from the span. Except where otherwise indicated, it is considered that (a) the vehicle has no vertical or angular motion at the instant it enters the span and (b) the bridge is initially at rest, and its surface is horizontal and perfectly smooth. In other words, the bridge is assumed to be cambered for dead-load deflection.

Bridges Considered

The bridges considered in this study correspond to type SA-2-53 in the Standard Bridge Plans of the Bureau of Public Roads (9). These bridges are of the I-beam type with steel girders and a concrete deck, designed for an H20-S16 loading. Their weights and natural frequencies, calculated from the data given in the standard plans, are listed in Table 1. In determining the natural frequencies, the bridges were assumed to behave as simply supported beams. The flexural rigidity of the bridge cross-section, EI,

was determined by considering noncomposite action between the slab and the beams, and the modular ratio for concrete was taken equal to 10.

TABLE 1

ESTIMATED WEIGHTS AND NATURAL FREQUENCIES OF SA-2-53 BRIDGES

Span (ft)	Total Weight (lb)	Fundamental Natural Frequency (cps)
20	98,000	12.13
45	227,000	5.41
50	257,200	4.97
60	323,500	4.08
70	385,700	3.19
78	448,200	2.81

For this class of bridges, the relationship between the speed parameter, α, defined by Eq. 1, and the speed of the vehicle, v, is given approximately by the equation

$$\alpha = 0.003\ v \tag{3}$$

in which v is in miles per hour.

Vehicles Considered

Three vehicles, A, B, and C, were used in this study. Their characteristics are shown in Table 2. The majority of the numerical results presented were obtained with Vehicle A. The characteristics of this vehicle were estimated from information obtained from 6 major truck and trailer manufacturers and from data contained in Reference 10. The front and rear axle of this vehicle are intended to represent the rear axle of a tractor and the axle of a semitrailer, respectively.

TABLE 2

CHARACTERISTICS OF VEHICLES USED

Quantity	Vehicle A		Vehicle B with Two Identical Axles	Vehicle C with Single Axle
	Front Axle	Rear Axle		
Unsprung weight (lb)	5,200	3,400	4,300	5,100
Sprung weight (lb)	26,800	28,600	27,000	26,000
Spring constant (lb/in.)	21,700	26,000	23,850	21,700
"Natural frequency" (cps)	2.81	2.98	2.90	2.86
Axle spacing (ft)	27.1		14.0	---
Polar moment of inertia of total sprung mass about centroid (kip-ft^2)	10,200		2,700	---
Gross vehicle weight (lb)	64,000		64,000	31,000

Vehicle B, with identical axles, is a simplified version of Vehicle A. The weight and spring constants for each axle of this vehicle were taken equal to the average values of the corresponding quantities for the two axles of Vehicle A. In this case, it

can readily be shown that the actual natural frequency of vibration of the vehicle for both the vertical mode and the pitching mode are identical and numerically equal to the natural frequencies of the axles.

Vehicle C, a single-axle loading, simulates the front axle of Vehicle A. This vehicle was used to obtain most of the data relating to the effects of deck unevenness.

The vehicle speeds used in this study ranged approximately from 15 to 70 mph.

RESULTS OF STUDY

Representative History Curves

It is instructive to examine first the response of a particular section of a bridge to the crossing of a vehicle. The graph of this response as a function of time will be referred to as a "history curve." Such curves are given in Figures 2 and 3.

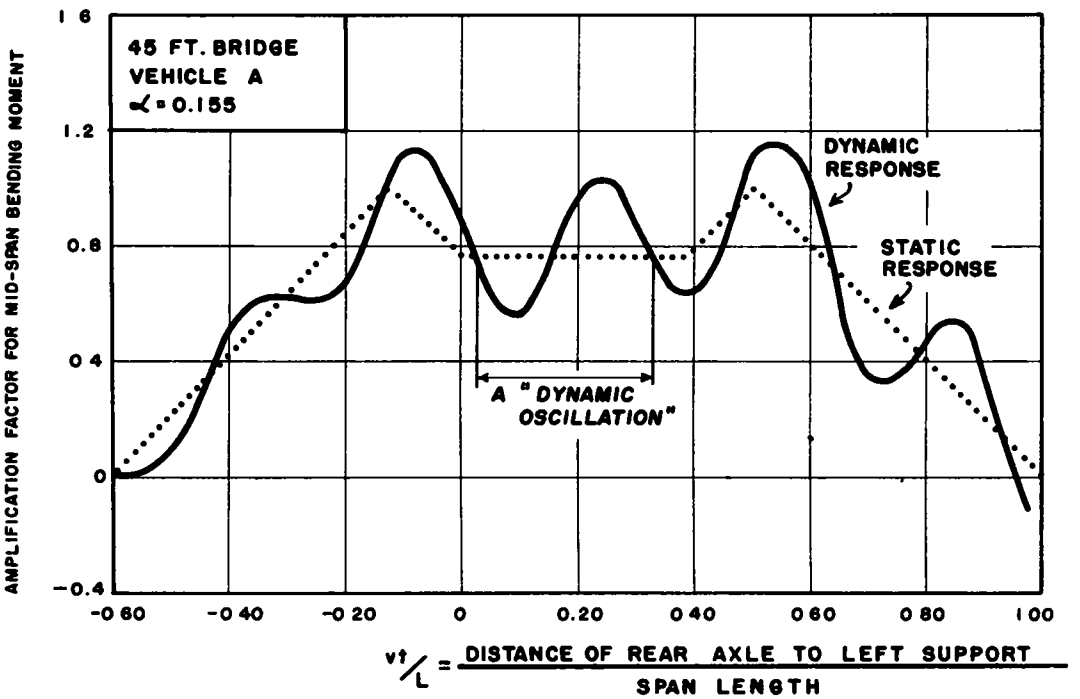

Figure 2. Representative history curves for midspan bending moment.

In Figure 2 the solid line shows the time history of the bending moment at midspan of a 45-ft bridge traversed by Vehicle A at a speed of 51 mph. The ordinate represents the amplification factor for moment at midspan, as previously defined, and the abscissa represents the quantity vt/L, in which t is time. Since both v and L are constant for a given problem, the abscissa is essentially a time coordinate. The time origin, t = 0, is taken as the instant when the rear axle enters the span. Accordingly, the time interval between the entry of the front axle on the span and the exit of the rear axle corresponds to a range of the abscissa from -s/L to unity. The symbol, s, denotes the spacing of the axles. For the case considered, s/L = 27.1/45 = 0.60.

Included in Figure 2 as a dotted line is the history curve of the corresponding static bending moment. This is essentially an influence line for moment at midspan due to the two-axle vehicle load. The difference between the ordinates of the solid curve and the dotted curve represents the history of the dynamic effect of midspan.

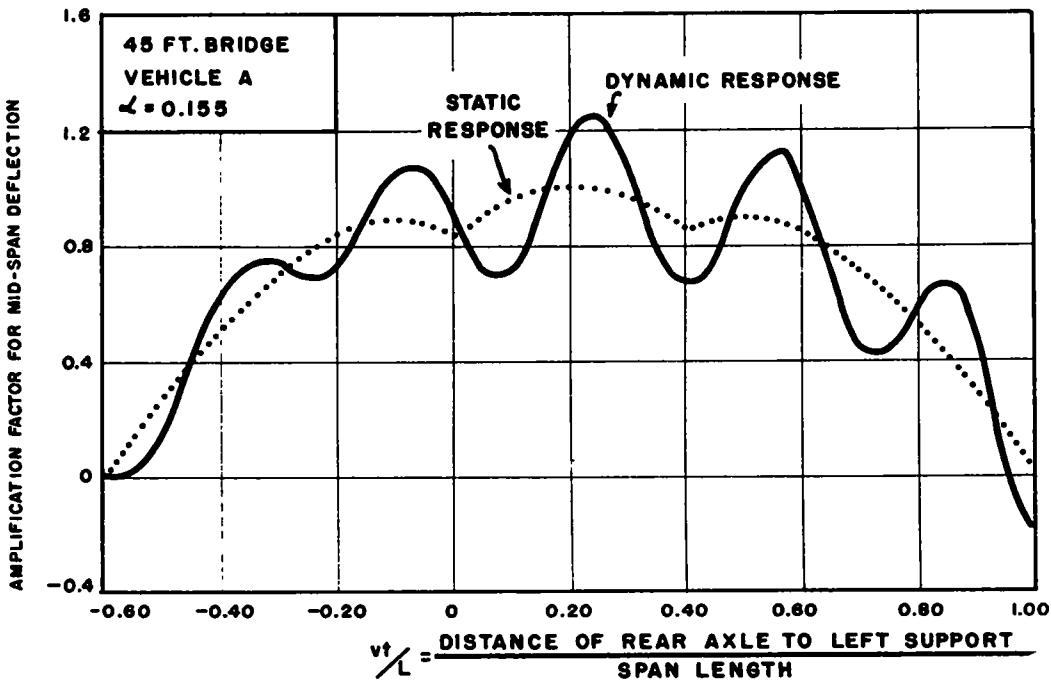

Figure 3. Representative history curves for midspan deflection.

Figure 3 shows the dynamic and static history curves for deflection at midspan for the particular bridge-vehicle system considered in Figure 2. As before, the ordinates are expressed as amplification factors.

It can be seen from Figures 2 and 3 that the dynamic history curves oscillate about the static curves with a "period" close to the fundamental natural period of vibration of the unloaded bridge, T_b. One complete wave on a history curve will be referred to as a dynamic oscillation. The reason the "period" of the dynamic oscillations is not identical to T_b is that the reactions between the axles and the bridge surface are not constant but vary with time generally in a fairly complex manner. If the "periods" of the individual waves are considered to be identical to T_b, then the speed parameter acquires an interesting physical meaning: its reciprocal

$$\frac{1}{\alpha} = 2\frac{L/v}{T_b} \tag{4}$$

is equal to twice the number of oscillations performed by the bridge in the time required for one axle to cross the span.

Both the ordinate and the slope of the dynamic response curves in Figures 2 and 3 are zero at the instant the front axle of the vehicle enters the span. This is as it should be, because the bridge is initially at its position of static equilibrium. The free vibration of the bridge (i.e., the motion after the vehicle has left the span) is determined by the values of the deflection and velocity of the bridge at the instant the rear axle leaves the span. From Figure 3 it can be seen that both of these quantities are different from zero in this case.

It should be noted that the maximum dynamic response may be greater or smaller than the maximum static response depending essentially on the positions of the dynamic oscillations relative to that of the maximum static response. The term "dynamic response" refers to the sum of the static effect and the dynamic effect. For a given amplitude of dynamic oscillation, the dynamic response will be greatest when the peak of a dynamic oscillation

coincides with the peak static response; it will be smallest when the valley point of a dynamic oscillation coincides with the peak static response. While the position of the load producing the maximum static effect at a section is fixed, the position of the dynamic oscillations is altered when the speed of the vehicle, its initial conditions, or the initial conditions of the bridge are changed.

Effect of Vehicle Speed

The numerical results showing the effects of the various factors will be presented, in general, in the form of spectrum curves. A spectrum curve is a plot of the maximum dynamic response as a function of some parameter of the bridge-vehicle system.

Figure 4 shows spectrum curves of amplification factors for midspan bending moment and midspan deflection as functions of the speed parameter for the system considered in the preceding section; i.e., the 45-ft bridge traversed by Vehicle A. In addition to the values of α the abscissa shows the speed of the vehicle in miles per hour. The ordinates of these curves at v = 51 mph are the maximum values of the corresponding curves in Figures 2 and 3.

It is noted that these spectrum curves are undulatory and that both the length and the height of the undulations increase with increasing values of the speed parameter. The undulatory feature is a consequence of the characteristics of the dynamic history curves, as discussed in the preceding section. It has been pointed out that the magnitude of the maximum dynamic response at a section depends on the position of the dynamic oscillations in the history curve relative to that of the maximum static value. An increase in the speed parameter, α, decreases the number of oscillations that the bridge undergoes while the vehicle is on the span. In other words, as the speed parameter increases, the lengths of the individual waves in the history curve increase, and the peaks of these waves shift to the right. It is this change in the position of the dynamic oscillations relative to that of the maximum static response that produces the major change in the magnitude of the maximum dynamic effect at a section.

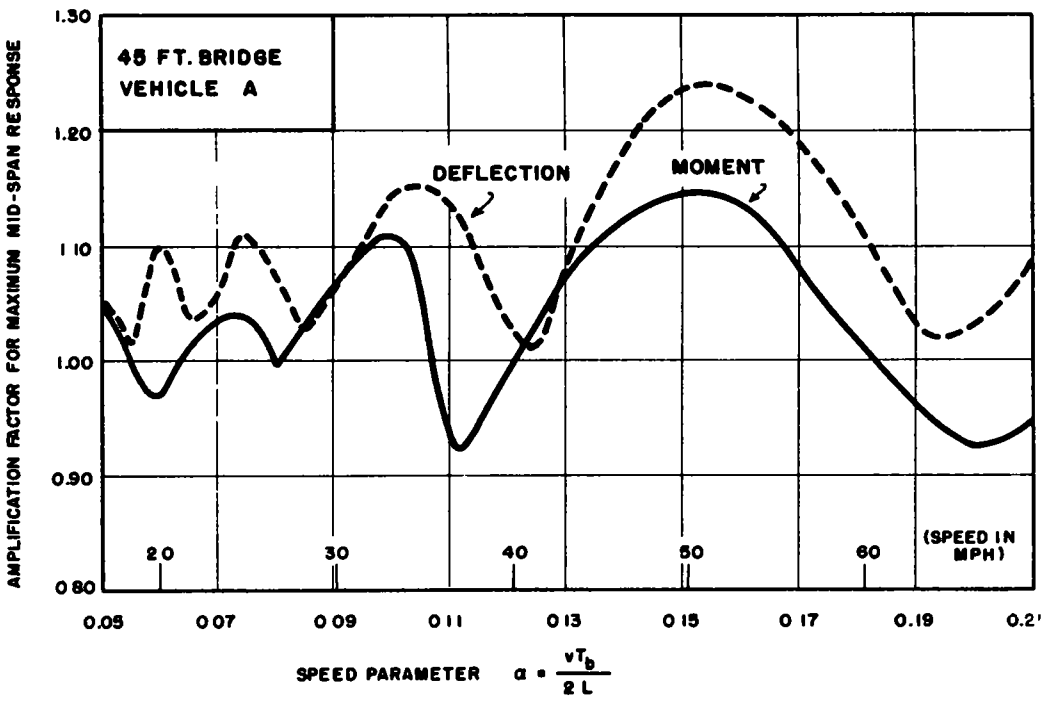

Figure 4. Effect of vehicle speed on maximum response at midspan.

The length of one undulation on the spectrum curve denotes the change in α necessary to "shift" one complete dynamic oscillation in the corresponding history curve past the position of the maximum static response. A relative maximum is obtained when the maximum static response coincides with the maximum ordinate of a dynamic oscillation, and a relative minimum is obtained when the peak static ordinate combines with the minimum ordinates of a dynamic oscillation.

Because the number of dynamic oscillations for the period that the vehicle is on the span is approximately inversely proportional to the speed parameter (see Eq. 4), a given change in speed will alter the positions of the dynamic oscillations by a smaller amount at high speeds than at low speeds. It is for this reason that the lengths of the undulations in the spectrum curves of Figure 4 increase with increasing speed.

The undulating nature of the spectrum curves, though interesting, is of a limited practical importance, because in practice the speed of a vehicle may vary within a fairly wide range. From the standpoint of application to design, it is the peak values of these curves that are significant. In this connection, it is important to note that the peak values of the response increase with increasing speed.

Figure 5 represents spectrum curves for midspan bending moment for the 20- and 70-ft spans together with the curve for the 45-ft span reproduced in Figure 4. The term "spectrum curve for bending moment" is used in lieu of the more precise term of "spectrum curve of amplification factors for bending moment" for the sake of brevity. This abbreviation will be adopted throughout the remaining part of this paper. Furthermore, unless otherwise noted, all bending moments will refer to midspan moments.

The differences in the curves in Figure 5 reflect essentially the influence of the bridge characteristics. It should be noted that when the span of the bridge is changed, both the weight ratio and the frequency ratios of the system are altered. The values of these parameters for the three spans may be determined from the data listed in Tables 1 and 2.

It is seen that the curves from the 20- and 70-ft spans exhibit the same general trends as those previously discussed for the 45-ft span. However, the magnitudes of the response for the 20-ft span are considerably larger than those for the longer spans. From available data (2) it would appear that the dynamic effects would not have been so large had a single-axle load been used to represent the vehicle.

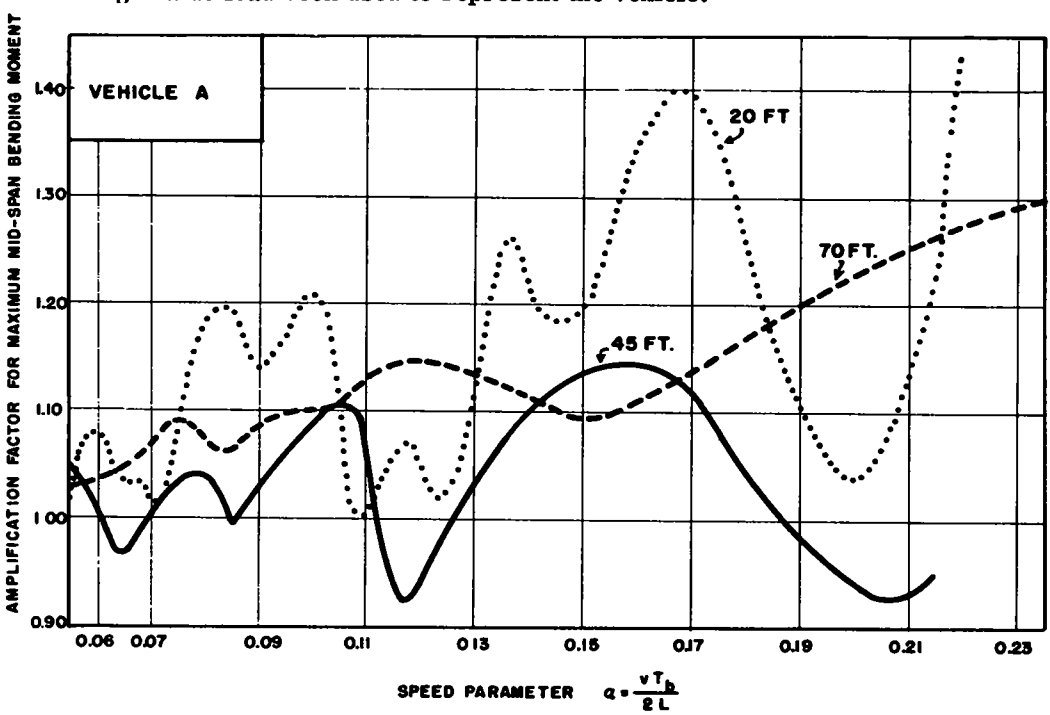

Figure 5. Effect of vehicle speed (for three span lengths).

For values of α less than 0.21, corresponding to vehicle speeds of less than about 70 mph, the absolute maximum amplification factors for bending moment for the 20-, 45-, and 70-ft spans are 1.42, 1.15, and 1.29, respectively. The corresponding values of α are approximately 0.17, 0.16, and 0.21. The lowest amplification factor, applicable to the 45-ft span, is associated with the smallest value of the speed parameter. In this connection, it should be pointed out that the location of the peak values of the response in a spectrum curve is a function of the axle spacing. For different axle spacings, it is quite possible that the absolute maximum amplification factor for the 45-ft span may occur at a higher speed, in which case, the magnitude of the amplification factor may be considerably larger. The effect of the axle spacing is considered further in the next section.

For the same range of the speed parameter, the absolute maximum amplification factors for deflection at midspan of the 20-, 45-, and 70-ft spans are 1.67, 1.24, and 1.26, respectively. The maxima occur at approximately the same values of the speed parameter as those for the absolute maximum bending moment. The spectrum curves for deflection are not included here, but are available in Wen (11).

In Figure 5 it is of interest to note that the curve for the 20-ft span is considerably more sensitive to variations in the speed parameter than are the curves for the longer spans. For the purpose of explaining this trend, it may be assumed that the period of the bridge oscillations induced by the front axle of the vehicle is equal to the fundamental natural period of vibration of the bridge, T_b. Then the time interval between the entry of the two axles on the span is s/v, and the number of complete oscillations executed by the bridge in this time interval is

$$n_o = \frac{s/v}{T_b} \tag{5a}$$

By virtue of Eq. 1, this equation may also be written in the form

$$n_o = \frac{s}{2L\alpha} \tag{5b}$$

The quantity n_o is essentially a measure of the "phase" of the bridge oscillation at the instant that the rear axle enters onto the span. Since the response of the bridge is obviously a function of this initial "phase," any change that influences this quantity will have a corresponding influence on the magnitude of the response. From Eq. 5b it can be seen that, for a fixed value of s, the change in n_o resulting from a given change in α is greater for the shorter spans. It follows then that the response of the short spans should be more sensitive to variations in α than that of the long spans. This is in agreement with the trends shown in Figure 5.

Figure 6 shows spectrum curves for bending moments at sections beneath the axles for a 45-ft span traversed by Vehicle A. In this case the moments are normalized with respect to the absolute maximum value of the static moment beneath an axle. This reference moment, which is the same for both axles because the two axle-loads are identical, represents the maximum possible static moment in the bridge.

It can be seen in this figure that the curve for the rear axle exhibits higher peaks and is more sensitive to variations in the speed parameter than the curve for the front axle. These features are consequences of the fact that the bridge is already in a state of oscillation when the rear axle enters the span, and may be explained in a manner analogous to that used previously in this section.

Effect of Axle Spacing

The field tests reported by Foster and Oehler (4) have shown that the axle spacing of the vehicle (in combination with the vehicle speed) is one of the major factors that influence the dynamic behavior of highway bridges. In these tests, relatively large dynamic effects in the bridge were observed when the time interval between the passing of the two axles over a given point was equal to the natural period of vibration of the structure. This observation suggests that the successive applications of the axle loads

may act as a periodic forcing agent on the structure and, therefore the synchronization of the period of vibration of the bridge with the period of load application may lead to a sort of "resonant" condition.

The time interval between the passing of the two axles of the vehicle over the same point is s/v. One would expect the "resonant" or "critical" condition to occur when

$$\frac{s/v}{T_b} = \frac{s/2L}{\alpha} = \text{an integer} \qquad (6)$$

This theory is generally borne out by the analytical results that have been obtained, covering three span lengths of 20, 45, and 70 ft, three vehicle speeds of approximately 35, 52, and 68 mph, and axle spacings from 0 to 35 ft. Some of these results are presented and discussed in the following paragraphs.

Figure 7 shows spectrum curves for moment and deflection as a function of the axle spacing. These results are for the 45-ft span and for a value of $\alpha = 0.105$ ($v \simeq 35$ mph). The characteristics of the vehicle used are the same as those of Vehicle A, except that the axle spacing is varied over a range. The abscissa shows both the dimensionless axle spacing parameter, s/2L, and the axle spacing, in feet. It is seen that the distances between consecutive peaks in these curves are approximately constant. Furthermore, the peaks occur at values of s/2L that are essentially multiples of the speed parameter used. In other words, Eq. 6 is satisfied quite closely. However, the magnitude of the peak effects are not sufficiently large to justify the use of the term "resonance" to describe the phenomenon. In the following, the term quasi-resonance will be used.

Spectrum curves of bending moment for the 20- and 70-ft spans are given in Figure 8, in which is also reproduced the moment spectrum curve from Figure 7. All three curves are for the same loading and the same value of the speed parameter, $\alpha = 0.105$. It can be seen that the general features of these curves are essentially the same. Additional curves, obtained for values of $\alpha = 0.155$ and 0.205, show the same characteristics. Some of these data are summarized in Table 3. The complete curves are available in Wen (11).

The third column of Table 3 lists the absolute maximum amplification factors for midspan moment for the complete range of axle spacings considered. The fourth column gives the amplification factors for s = 0; i.e., a single axle having the same total load.

TABLE 3

SUMMARY OF MAXIMUM MOMENTS FOR A RANGE OF AXLE SPACINGS

Span Length (ft)	α	Amplification Factor for Maximum Midspan Moment	
		Maximum Value for $0 \leq s \leq 35$	Value for s = 0
20	0.105	1.17	0.96
	0.155	1.31	1.06
	0.205	1.34	0.84
45	0.105	1.18	1.00
	0.155	1.27	1.16
	0.205	1.32	0.97
70	0.105	1.11	1.02
	0.155	1.21	1.01
	0.205	1.18	1.03

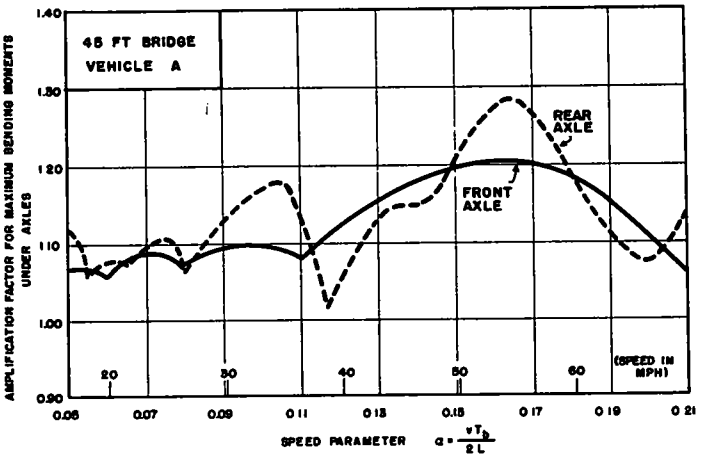

Figure 6. Effect of vehicle speed on maximum bending moments under axles.

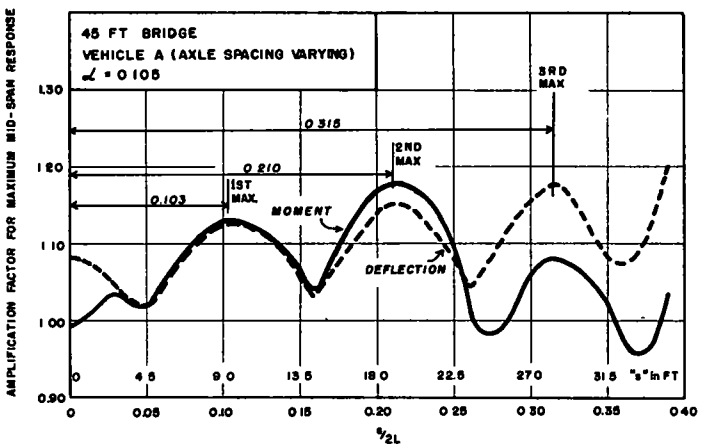

Figure 7. Effect of axle spacing (45-ft bridge).

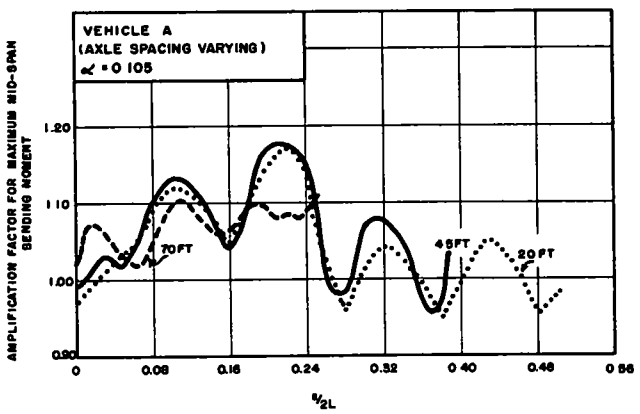

Figure 8. Effect of axle spacing (for three span lengths).

It is seen that the absolute maximum effects are, in general, significantly larger than those for the single-axle loading. However, this comparison is not a reliable measure of the effect of axle spacing, because the results for the single-axle load are quite small for the particular speeds considered. A change in the speed parameter will affect both sets of values, but the possible increase in the magnitude of the effects is expected to be more pronounced in the case of the single-axle load. This may be appreciated by noting that for the 20-ft span the amplification factor is less than one, even for a value of the speed parameter as high as $\alpha = 0.205$. It is apparent that in this case the maximum static moment combines with a negative ordinate of a dynamic oscillation. The amplitude of this oscillation is at least 0.16; i.e., 16 percent of the maximum static moment. Therefore, the amplification factor for moment will increase at least by 0.32 when the speed of the vehicle is changed so that the peak static moment combines with the maximum positive ordinate of a dynamic oscillation. For a complete evaluation of the axle-spacing parameter, one must consider also the effect of varying the speed parameter.

Table 4 shows the interrelationship of speed and axle spacing. Column 1 gives the peak values of the bending moment obtained by keeping the axle spacing at $s = 27.1$ ft and increasing the speed parameter to a maximum value of 0.21. Column 2 gives the corresponding values obtained by considering three values of the speed parameter, as previously noted, and varying the axle spacing from 0 to 35 ft. It can be seen that, whereas for the 20- and 70-ft spans, the values given in Column 1 are larger than those in Column 2, for the 45-ft span the reverse is true. In Column 3 are listed the larger of the values given in Columns 1 and 2. These results show that the peak dynamic effects increase with decreasing spans.

TABLE 4

SUMMARY OF MAXIMUM MOMENTS FOR A RANGE OF SPEEDS AND AXLE SPACINGS

Span (ft)	Maximum Amplification Factors for Midspan Moment		
	(1) Speed Varied	(2) Axle Spacing	(3) Max. Value of (1) and (2)
20	1.42	1.34	1.42
45	1.15	1.32	1.32
70	1.29	1.21	1.29

From the results presented, it may be inferred that, for a vehicle having more than two axles, the dynamic effects produced by the individual axles may be cumulative, if the spacings between consecutive axles are multiples of one another.

Concerning the relative magnitude of the dynamic effects produced by tandem axles and a single axle of the same total load, it may be noted that, no matter how small the axle spacing, Eq. 6 can always be satisfied, provided the vehicle speed is sufficiently low. However, from the discussion presented relative to the effect of vehicle speed, it follows also that quasi-resonance at low speeds is not as important as at high speeds. If one somewhat arbitrarily takes $v \cong 33$ mph as the lowest speed for which dynamic effects are of consequence, and uses $s = 4$ ft for tandem axles, then he finds that Eq. 6 can be satisfied only for spans equal to or less than 20 ft. That is, for vehicle speeds greater than about 33 mph, the quasi-resonant condition cannot be realized in bridges with spans longer than 20 ft. Hence, as one might expect intuitively, the dynamic effects produced by tandem axles may be substantially larger than those produced by a single axle only in the case of very short spans.

Effect of Initial Bridge Motion

The dynamic oscillations induced by the passage of a vehicle over a bridge may last for a considerable time after the vehicle has left the span. The influence of this motion must be considered in evaluating the response of the bridge to the passage of a second vehicle following the first closely.

It is reasonable to assume that the initial oscillation is in the fundamental mode of vibration of the bridge. The initial deflection, $y(x, t')$, may then be expressed by the equation

$$y(x, t') = y_o \sin\frac{\pi x}{L} \sin(2\pi\frac{t'}{T_b} + \beta_b) \tag{7}$$

in which y_o is the amplitude of the midspan deflection, x is the position coordinate measured from the left support, t' is time measured from the instant the front axle enters the span, and β_b is a phase angle. At t' = 0, the midspan deflection is $y_o \sin\beta_b$, and the corresponding velocity is $\frac{2\pi}{T_b} y_o \cos\beta_b$. The initial condition of the bridge may be specified either in terms of the initial deflection and velocity, or in terms of the amplitude y_o and the phase angle β_b. In the following, the latter alternative is used. For convenience, the amplitude y_o is specified by the dimensionless parameter

$$q_b = y_o/y_s \tag{8}$$

in which y_s is the maximum static deflection of the bridge at midspan due to the weight of the vehicle.

The influence of the phase angle, β_b, on the response of the bridge is shown in Figure 9, in which are given spectrum curves of bending moment for a 45-ft bridge traversed by Vehicle A. The value of $q_b = 0.314$. The three curves correspond to vehicle speeds of 38, 51, and 58 mph. Values of $\beta_b = 0$ and $\beta_b = 2\pi$ define the condition in which the beam has no initial deflection but has a maximum downward velocity. For $\beta_b = \pi$ there is no initial deflection, but there is a maximum upward velocity. For $\beta_b = \frac{\pi}{2}$ there is an initial maximum downward deflection but no initial velocity.

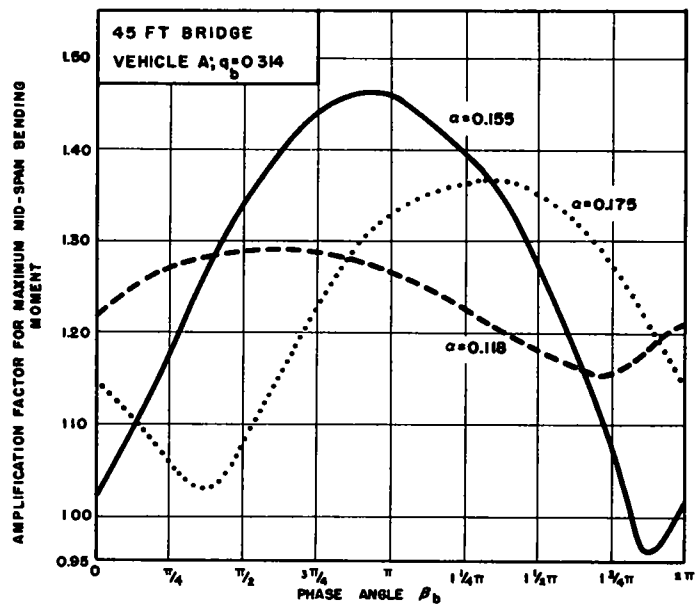

Figure 9. Effect of phase angle of bridge initial oscillation.

It can be seen from this figure that the maximum response at midspan is quite sensitive to variations in the phase angle β_b. As might be expected, the peak values of the response, which are the most significant quantities from a design standpoint, occur at different values of β_b for the different speeds.

In Figure 10 the absolute maximum values of the bending moment and deflection for three initially oscillating bridges are plotted as a function of the initial oscillation parameter q_b. These results are for Vehicle B and a speed parameter of $\alpha = 0.10$. The amplification factors plotted are the maximum possible for values of the phase angle β_b in the range between 0 and 2π. In other words, the ordinates in this plot represent the peaks of curves similar to those presented in Figure 9.

It can be seen from Figure 10 that the amplification factors for both moment and deflection increase linearly with q_b and that the rate of increase is approximately one to one. Accordingly, the maximum effects produced by a vehicle in an initially oscillating bridge are approximately equal to the sum of the effects of the initial oscillation and the effects produced by the vehicle when the bridge is initially at rest. This result may be expressed by the equation

$$(AF)_{q_b} = (AF)_0 + q_b \qquad (9)$$

in which $(AF)_{q_b}$ is the maximum possible amplification factor for either moment or deflection at midspan for an initially oscillating bridge, and $(AF)_0$ is the corresponding quantity for the bridge when initially at rest.

In Table 5, the amplification factors for bending moment predicted by Eq. 9 are compared with the exact values as determined from the plots given in Figures 9 and 10. It can be seen that the agreement between the two sets of results is quite satisfactory. It should be pointed out, however, that additional solutions are required to establish the range of validity of Eq. 9.

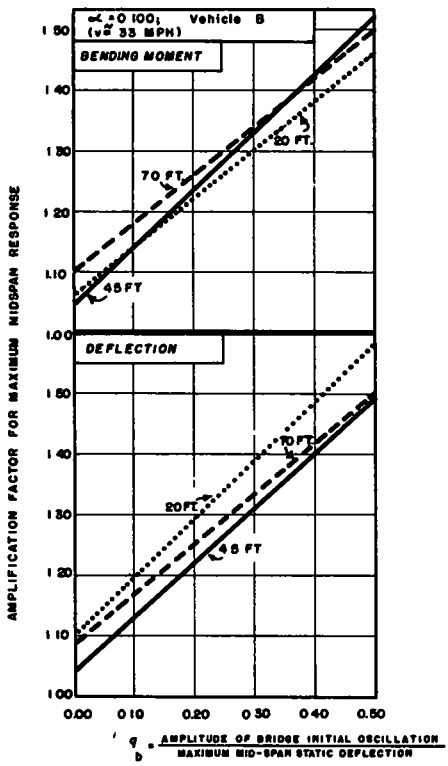

Figure 10. Effect of amplitude of bridge initial oscillation.

TABLE 5

COMPARISON OF EXACT AND APPROXIMATE VALUES OF MAXIMUM MOMENT

α	Maximum Amplification Factor for Midspan Moment		
	$q_b = 0$	$q_b = 0.314$	
		From Fig. 9	From Eq. 9
0.118	0.97	1.29	1.28
0.155	1.15	1.46	1.46
0.175	1.04	1.37	1.35

Span (ft)	Maximum Amplification Factor for Midspan Moment		
	$q_b = 0$	$q_b = 0.50$	
		From Fig. 10	From Eq. 9
20	1.06	1.46	1.56
15	1.05	1.52	1.55
70	1.10	1.50	1.60

Effects of Initial Vehicle Motion

The influence of this factor is investigated by assuming that the initial motion of the vehicle corresponds to one of its natural models of vibration. Proceeding in a manner analogous to that used in the preceding section, it can be shown that, for each motion, the initial condition of the vehicle can be specified in terms of the amplitude of the motion and a phase angle.

For the motion corresponding to the vertical or bouncing natural mode of vibration, the phase angle will be denoted by β_v, and the amplitude of the initial displacement will be expressed in terms of the dimensionless parameter, q_v, defined as

$$q_v = z_o/z_s \tag{10}$$

where z_o is the amplitude of the dynamic vertical displacement of the centroid of the sprung mass, measured from the position of static equilibrium, and z_s is the corresponding static deflection. The maximum value of q_v measured in the field (3, 12) appears to be on the order of 0.40. For the motion corresponding to the pitching or angular natural mode of vibration, the phase angle will be denoted by β_p, and the amplitude of the motion will be expressed in terms of the parameter, q_p, defined as

$$q_p = u_o/u_s \tag{11}$$

where u_o is the amplitude of the angular displacement, and u_s is the ratio of the sum of the static deformations of the springs for the two axles divided by the spacing of the axles.

The effects of the phase angles, β_v and β_p, on the response of the bridge are similar to that of the phase angle for initial bridge oscillation, β_b, considered in Figure 9, and they will not be discussed further here.

The effects of the amplitudes of initial motion are shown in Figure 11, wherein are given spectrum curves for bending moment and deflection for a 70-ft bridge traversed by Vehicle B at a speed corresponding to a value of $\alpha = 0.10$. For the solid curves the initial oscillation consists of a purely vertical motion, and for the dashed curves it consists of a purely angular motion. The ordinates in these plots represent the absolute maximum amplification factors for all possible values of the phase angle associated with the initial motion considered.

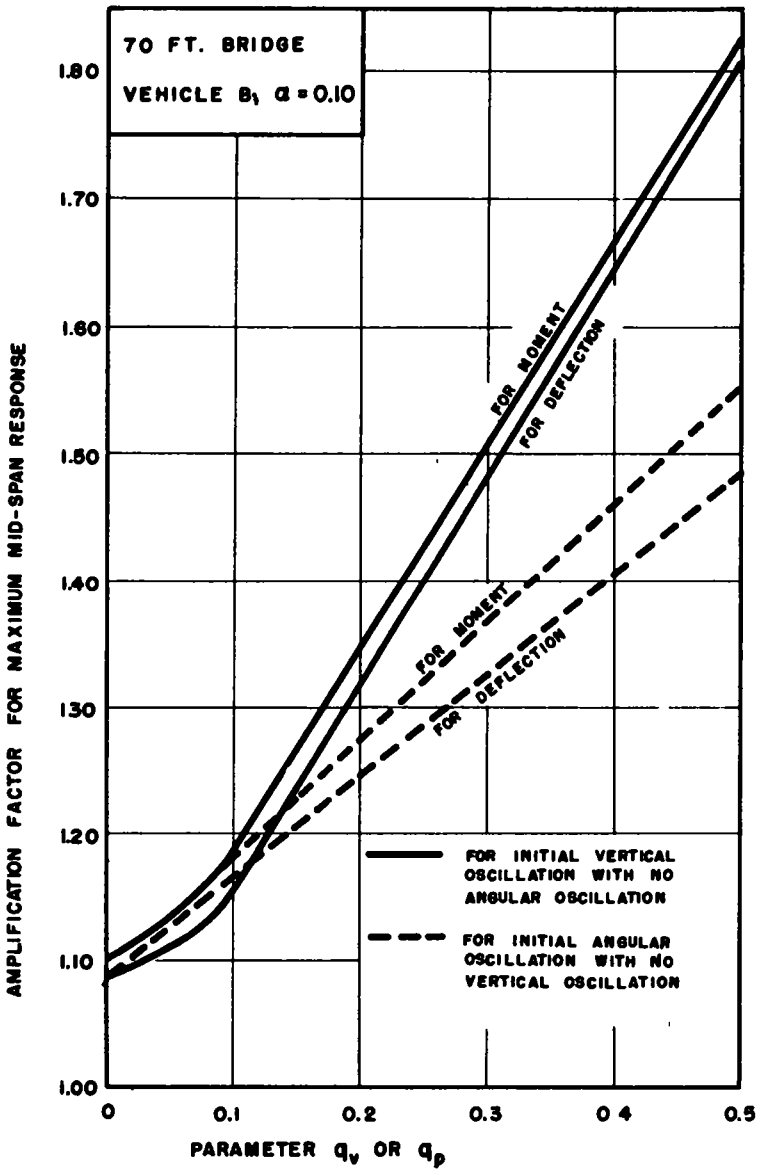

Figure 11. Effect of amplitude of initial oscillation of vehicle.

It is seen that, except for the initial portions of the solid curves that are curved, these curves increase linearly with increasing values of the abscissae. This linear relationship between the maximum response and the amplitude of the initial vehicle oscillation has been noted before (3) for the case where the vehicle was represented as a single-axle load.

For the vehicle considered, equal values of q_v and q_p define equal amplitudes of dynamic deformation for the springs of the two axles. Of course, the deformations of the individual springs are in phase for the bouncing motion and 180 deg out of phase for the pitching motion. On comparing the magnitudes of the dynamic effects produced for

identical values of q_v and q_p, one finds that, when q_v and q_p are greater than about 0.10, the effects for an initial bouncing motion are appreciably larger than those for an initial pitching motion. It should be pointed out, however, that the characteristics of the vehicle used to obtain these data are such that the two natural frequencies are equal. It is conceivable that, if the two frequencies are appreciably different from one another and the pitching frequency is closer to the natural frequency of the bridge than is the bouncing frequency, the maximum effects produced by the initial pitching motion may be greater than those due to the initial bouncing motion.

For the range of amplitudes of initial vehicle oscillation considered in Figure 11, the maximum amplification factors for the bouncing and pitching motion are roughly 1.8 and 1.5, respectively. These are undoubtedly rather large dynamic effects. However, it should be remembered that in obtaining these results the vehicle has been assumed to have no damping. The effect of damping will be to reduce the magnitude of the amplification factors. This reduction is expected to be particularly significant for the longer spans for which the time required for the vehicle to cross the span at a given speed is greater than for the shorter spans.

Effect of Deck Unevenness

The fact that the condition of the bridge surface may be one of the major factors controlling the magnitude of the dynamic effects in highway bridges was demonstrated in the tests reported by Edgerton and Beecroft (7). These tests involved two bridges with identical superstructures, except that one bridge had a smoother deck than the other. For the same loading, considerably greater dynamic effects were measured in the bridge with the uneven deck.

The majority of the solutions presented in the following paragraphs are for a sinusoidal unevenness. The results of an exploratory study are also given for a deck profile representable by a series of half-sine waves of unequal lengths and amplitudes, and for a localized irregularity or a "bump" located on the otherwise smooth surface. The vehicle is represented as a single-axle load.

Sinusoidal Unevenness. — Let p(x) denote the deviation of the deck profile from the design grade, as shown in Figure 1. Then a sinusoidal unevenness may be expressed by the equation

$$p(x) = b \sin \frac{m\pi x}{L} \tag{12}$$

in which b is the amplitude of the unevenness, and m is the number of half-sine waves along the span. The length of each half-sine wave is L/m.

There are two conditions under which the dynamic effects produced by the unevenness may be expected to be of appreciable magnitude. The first corresponds to the case in which the period of the profile deviation, T_p, is equal or close to the natural period of vibration of the vehicle, T_v. The period T_p is equal to the time required for the vehicle to travel the distance covered by one complete wave, and it is given by the equation

$$T_p = \frac{2L/m}{v} = \frac{1}{m}\frac{T_b}{\alpha} \tag{13}$$

By equating the expression on the right-hand side of this equation with T_v, one finds that this critical or "resonant" condition will occur when

$$m\alpha = \frac{T_b}{T_v} \tag{14}$$

It is seen that m and α are interrelated. That is, for a given value of m there is a critical speed, and for a given speed there is a critical value of m.

The second critical condition may be expected when the period of the profile variation coincides with the natural period of vibration of the bridge, T_b. On equating these two periods one obtains the relation

$$m\alpha = 1 \tag{15}$$

Although the amplitude of variation of the force exerted by the vehicle on the bridge may be small in this case, the dynamic effects in the bridge may still be appreciable. The absolute maximum effects might be expected to occur when

$$T_p = T_v = T_b$$

In this case Eqs. 14 and 15 are identical.

In the formulation of Eqs. 14 and 15, it has implicitly been assumed that there is no coupling between the motion of the vehicle and the bridge. The extent to which these approximate equations can predict the actual critical conditions is discussed in the following.

Figure 12 gives spectrum curves for bending moment as a function of the speed parameter for values of m = 5, 9, and 15. Included in this figure as a solid curve is also the solution for a smooth surface, b = 0. The bridge involved is the 70-ft span, and the vehicle is the single-axle Vehicle C. In this case, the amplitude of the unevenness, b, is one thousandth the length of the half-sine wave. Since L = 70 ft, the amplitude b, in inches, is given by the expression

$$b = \frac{0.84}{m}$$

in which m is different from zero.

For these and all subsequent problems the vehicle is assumed to have no vertical motion as it enters the span, and the bridge is considered to be initially at rest but deflected under its own weight. In other words, the design grade is considered to coincide with the dead-load deflection configuration of the structure. The first wave of the unevenness is assumed to be located below the design grade.

The most striking feature of the results depicted in this figure is that the peak values of the response for the wavy surfaces are considerably larger than those for the smooth surface. The values of α corresponding to the maximum peak values of the response are listed in Table 6 together with the values evaluated from Eqs. 14 and 15. In general the values obtained from Figure 12 are close to the predicted value, particularly those based on Eq. 14.

According to Eqs. 14 and 15, for each of the spectrum curves in Figure 12 there should be two high peaks. The fact that there is only one peak may be attributed to the closeness of the two resonant conditions that appears to have forced the two peaks to merge into one. For the system considered, the ratio $T_b/T_v = 0.90$. Additional results reported elsewhere (8)(13) indicate that large dynamic effects do occur for each of the two critical conditions referred to above, but of the two conditions, the condition

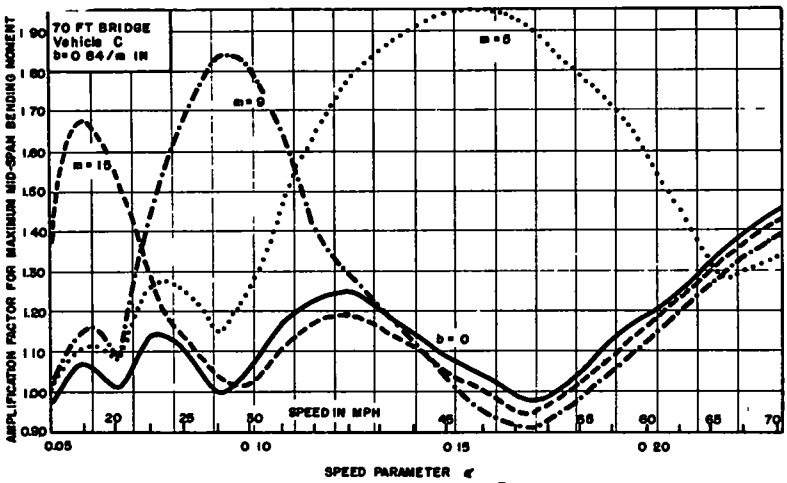

Figure 12. Effect of vehicle speed (bridge with sinusoidal deck profile).

of synchronization between the period of the profile variation and the natural period of vibration of the vehicle is, in general, the more severe. The implication of this result is that, in order for the dynamic effects in the bridge to be large, the amplitude of the variation of the interacting force must first be magnified.

In Figure 12 it is noted that the ordinates of the curves for the wavy surfaces decrease rapidly after they have passed their respective high peaks and eventually join the curve for the smooth surface. This is as it should be, inasmuch as one would normally expect the dynamic effect produced by the sinusoidal unevenness to be negligible when the period of the disturbance, T_p, is small in comparison with the period of the responding system. For a given bridge-vehicle system, T_v and T_b are constant but T_p is inversely proportional to v and m. Hence, the larger the value of m for a curve in Figure 12, the smaller is the value of v or α at which the dynamic effects of the unevenness become negligible and the curves for m = 0 to start to join the curve for b = 0.

TABLE 6

COMPARISON OF EXACT AND APPROXIMATE "CRITICAL" VALUES OF α

Value of m	Critical Value of α		
	From Fig. 12	From Eq. 14	From Eq. 15
5	0.154	0.179	0.200
9	0.093	0.100	0.111
15	0.057	0.060	0.067

In Figure 13 are given spectrum curves for bending moment for five different bridges as a function of the number of half-sine waves present along the span. In each case, the speed parameter is $\alpha = 0.1$ and the amplitude of the wave is

$$b = 0.001 \frac{L}{m}$$

The vehicle used is similar to Vehicle C, except that its natural period of vibration is 0.28 sec instead of 0.35 sec. The values in parentheses in this figure represent the ratio T_b/T_v.

The values of m corresponding to the two highest peaks of the curves in Figure 13 are compared in Table 7 with the values obtained from Eqs. 14 and 15. It can be seen that the agreement between the actual and the predicted critical values is quite satisfactory.

In Figure 13 it can be seen that, except for the 78-ft span, the magnitude of the peak response increases with increasing span length. This trend is due to two factors: (a) since the parameter mb/L is constant for all span lengths, the amplitude of the waves corresponding to a fixed value of m is greater for the longer spans and (b) as the span length increases the ratio T_b/T_v approaches unity, with the result that at the critical value of m the period of the surface unevenness is in synchronism with both the natural period of the vehicle and the natural period of the bridge. Of the two factors, the latter is the more dominant. This is evidenced by the fact that the curve for the 78-ft span, which has the largest value of b but a ratio of $T_b/T_v = 1.27$, lies considerably below the curves for the 60- and 70-ft spans.

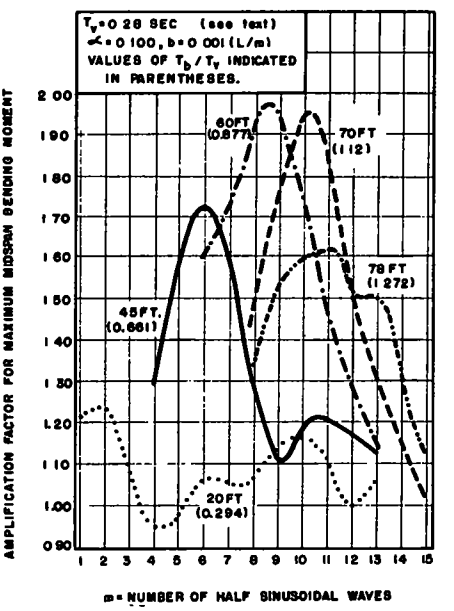

Figure 13. Effect of ratio T_b/T_v (bridges with sinusoidal deck profile).

TABLE 7

COMPARISON OF EXACT AND APPROXIMATE "CRITICAL" VALUES OF m

Span (ft)	$\frac{T_b}{T_v}$	Critical Value of m			
		From Fig. 13	From Eq. 14	From Fig. 13	From Eq. 15
20	0.294	2.0	2.9	10.0	10.0
45	9.66	6.0	6.6	10.7	10.0
60	0.875	8.8	8.7	8.8	10.0
70	1.12	10.4	11.2	10.4	10.0
78	1.27	13.0	12.7	11.0	10.0

It is important to note that although the amplitude of the surface unevenness considered in these conditions was by no means excessive, the computed effects are quite large. In this connection, it must be remembered that the effects of both bridge damping and vehicle damping were not accounted for in the analysis. Accordingly, the computed effects are generally larger than those expected in practical cases. The influence of damping is likely to be particularly important when the number of waves along the span is large or when the ratio T_b/T_v is close to unity.

Semisystematic Unevenness.—The form of the unevenness considered is shown in Figure 14. It consists of five half-sine waves, alternately of opposite signs, having different lengths and amplitudes. The length of each end wave is taken equal to 1/5 the length of the span, whereas the lengths of the remaining waves are varied over the entire possible range, keeping the waves symmetrical about the center of the span. The amplitude-to-length ratio is considered to be the same for all the waves.

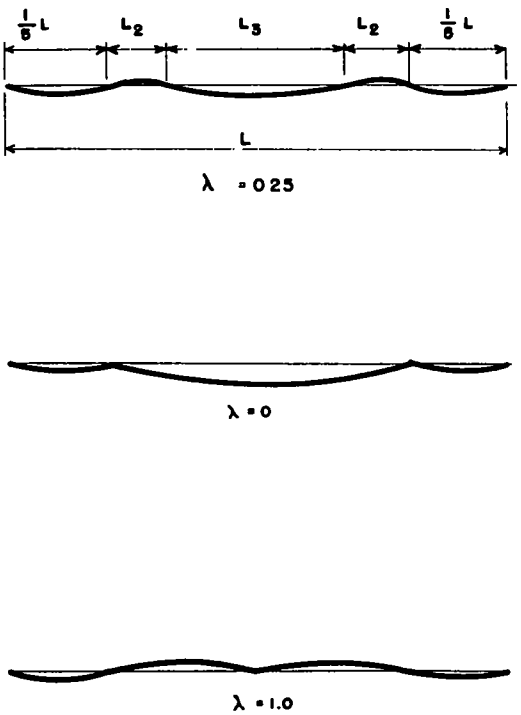

Figure 14. Sinusoidal deck profile with varying wave length.

The distribution of the unevenness can conveniently be specified in terms of the dimensionless parameter, λ, defined as

$$\lambda = \frac{L_2}{L_2 + L_3}$$

where L_2 and L_3 are the lengths of the second and third waves, respectively. The range of λ is from 0 to 1. As shown in Figure 14, λ = 0 corresponds to the case in which there are only three waves along the span, whereas λ = 1 corresponds to the cases in which there are four waves. For a sinusoidal unevenness λ = 0.5. The end waves are assumed to be located below the design grade.

The parameter λ is essentially a measure of the regularity of the unevenness. Its influence is shown in Figure 15, in which the absolute maximum amplification factor for midspan bending moment is plotted as a function of α for bridges of 20-, 45-, and 70-ft spans. The

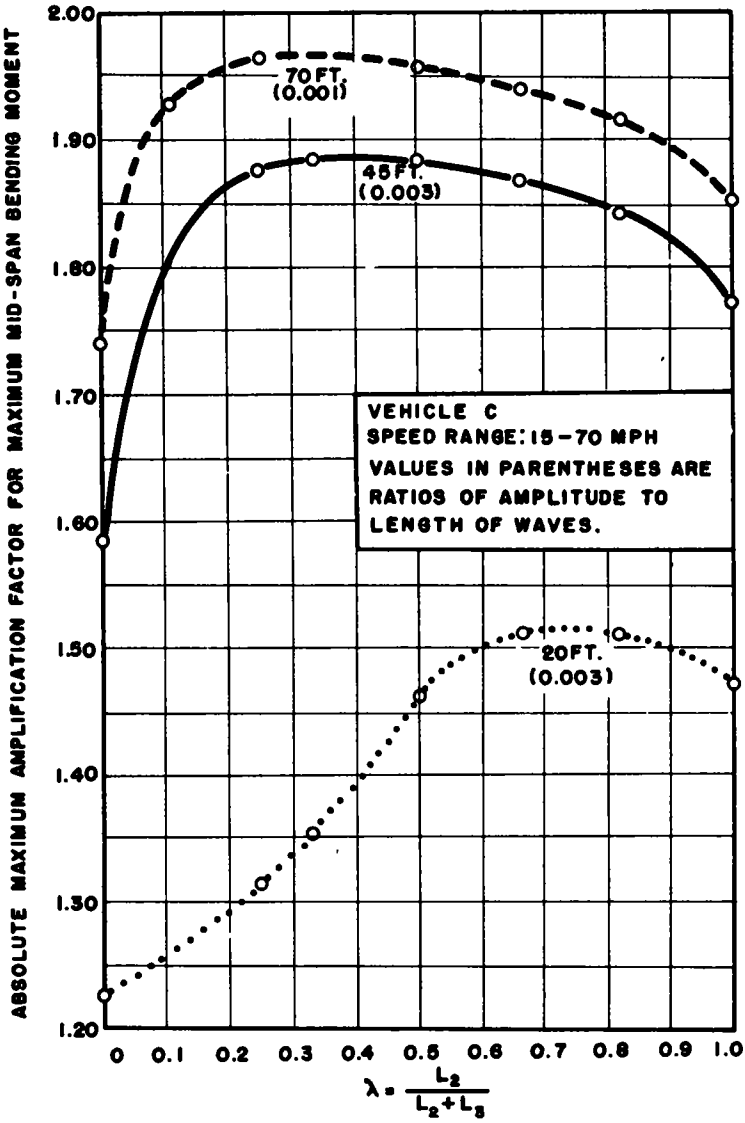

Figure 15. Effect of relative wave length.

amplification factors plotted are the maximum within the range of speeds from 15 to 70 mph. These results were obtained by use of Vehicle C.

It is noted that for a fairly wide range of values of λ the ordinates of the curves in this figure are of the same order of magnitude as the corresponding ordinate for a sinusoidal profile ($\lambda = 0.5$). This is particularly true in the case of the 70-ft span for which the natural period of the bridge and the vehicle are close to one another. For this span, the amplification factor for bending moment varies from 1.97 to 1.85 for values of the λ in the range between 0.15 and 1.0.

The practical implication of these results is that, even when the unevenness of the bridge deck is not entirely symmetric, it may be possible to estimate the absolute maximum effects by considering a sinusoidal unevenness with approximately the same number of waves and an amplitude equal to the average amplitude of the waves in the actual profile.

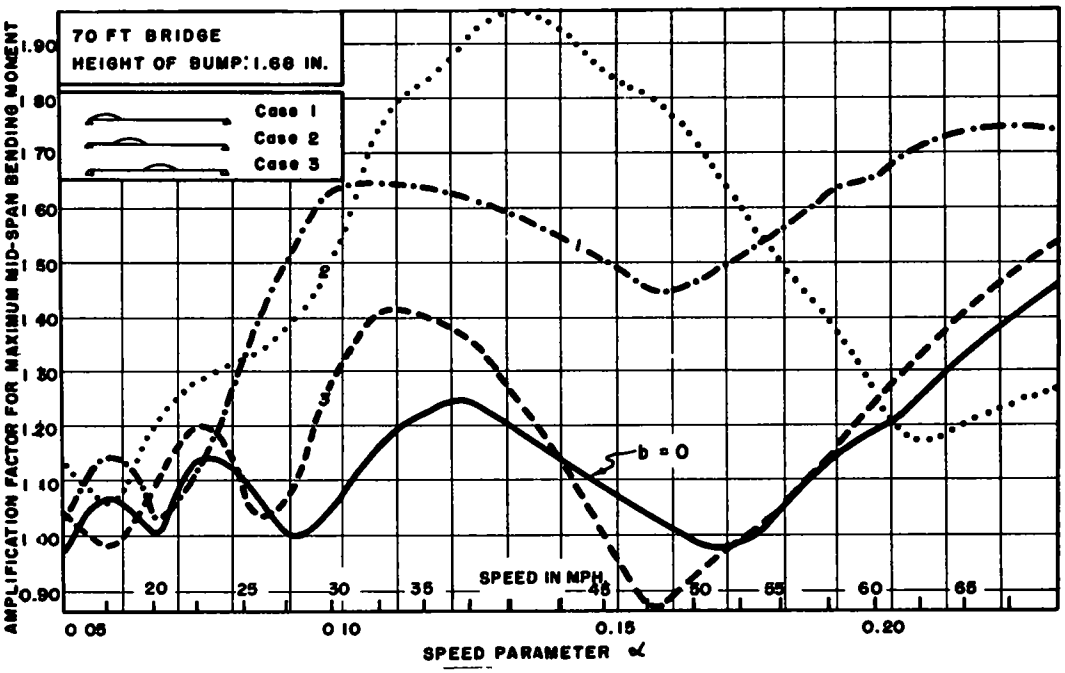

Figure 16. Effect of a "bump" on deck.

Localized Unevenness.—Figure 16 gives spectrum curves for bending moment as a function of the speed parameter for a 70-ft bridge with a localized irregularity in the form of a half-sine wave. The wave is considered to project above the design grade. Its amplitude is 1.68 in. and its length is 1/5 of the length of the bridge span. The curves labeled 1, 2, and 3 correspond to the cases where the irregularity occupies the first, second, and third fifth of the span, respectively. The curve labeled zero is for a smooth deck.

It is seen that the dynamic effects produced by the unevenness are in general of considerable magnitude, and the absolute maximum effect is produced when the irregularity is located at the second fifth of the span instead of when centered about midspan. The latter result can be explained as follows. The primary effect of the irregularity is to amplify the vertical motion of the vehicle and thus increase the magnitude of the dynamic reaction exerted by the vehicle on the bridge. But there is a time lag between the initiation of the motion of the vehicle due to the unevenness and the development of the maximum possible dynamic reaction. When the irregularity is situated at midspan, by the time the dynamic reaction attains its maximum value, the vehicle is past midspan and at a position for which a given force will stress the structure of the lesser extent than when the same force is applied at midspan.

SUMMARY

The results of an analytical study have been presented to illustrate the influence of some of the factors producing dynamic effects in simple-span highway bridges. In the majority of the solutions the vehicle was represented as a two-axle loading.

The factors considered fall into two categories. In the first belong the factors related to the behavior of bridges with a smooth surface traversed by a vehicle that is initially in its position of static equilibrium. They include the speed of the vehicle, the axle spacing, and the initial oscillation of the bridge. The common characteristics of these factors is that they prevail in all bridges to a comparable degree, and their possible ranges are reasonably certain. In the second category belong the additional factors associated with the effects of the unevenness of the bridge surface and the ap-

proaches. They include the initial oscillation of the vehicle and the characteristics of the bridge surface. The relative importance of these factors may be quite different for different bridges, as the surface irregularities depend on such factors as the type of the pavement, and the location and maintenance of the bridge. At the present time, little is known about the distribution and the magnitude of roadway unevenness for highway bridges.

In general the magnitude of the maximum dynamic effects in a bridge increase with increasing vehicle speed. For axle spacings larger than the bridge length, the dynamic effects produced by a two-axle loading were found to be larger than those produced by single-axle loading. The increase is attributed to the fact that when the rear-axle enters the span the bridge is already in a state of oscillation.

By varying the axle spacing while keeping all other variables constant, it was found that a quasi-resonance condition is developed when the time interval between the application of the two axles over a point is equal to the fundamental natural period of vibration of the bridge.

If the bridge is already in a state of oscillation when the vehicle enters the span, the dynamic effects produced by the vehicle depend on the timing of the entry of the vehicle with the oscillation of the bridge. The absolute maximum effect can be estimated approximately by superimposing on the maximum effect due to the initial oscillation the effect that would be produced by the vehicle if the structure were initially at rest.

The influence of the initial vehicle oscillation was investigated by considering both a bouncing and a pitching motion for the vehicle. For the problems studied it was found that, for the same amplitude of initial deformation in the springs, the effects of pitching are less severe than those of bouncing. The magnitude of the resulting dynamic effects were found to increase almost linearly with the amplitude of the initial oscillation considered.

The influence of the unevenness of the bridge deck was investigated by considering a sinusoidal profile variation, a semisystematic unevenness consisting of a series of half-sine waves of unequal amplitudes and lengths, and a localized unevenness. The results obtained show clearly that roadway unevenness may be a source of large dynamic effects in highway bridges.

In interpreting the practical significance of the solutions presented in this paper it must be kept in mind that the contributions of both vehicle damping and bridge damping were not accounted for in the analysis. Accordingly, the computed effects are generally larger than those to be expected in actual cases.

ACKNOWLEDGMENT

The study described in this paper was made as part of the Highway Bridge Impact Investigation, a research project conducted by the University of Illinois Engineering Experiment Station in cooperation with the Illinois Division of Highways and the Bureau of Public Roads, U. S. Department of Commerce. This paper is based in part on a doctoral dissertation by Wen (11) prepared in 1957. The data concerning the effects of roadway unevenness were drawn from Toledo-Leyva and Veletsos (13). The latter report is based on an M.S. thesis by Mr. Toledo-Leyva, formerly Research Assistant in Civil Engineering.

REFERENCES

1. "Deflection Limitations of Bridges." Progress Report, Committee on Deflection Limitations of Bridges. Jour. of the Structural Division, Proc. ASCE, 84, Paper 1633, (May 1958).
2. Tung, T. P., Goodman, L. E., Chen, T. Y., and Newmark, N. M., "Highway Bridge Impact Problems." HRB Bull. 124, 111 (1956).
3. Biggs, J. M. Suer, H.S., and Louw, J.M., "Vibration of Simple-Span Highway Bridges." Transactions ASCE, 124: 291 (1959)
4. Foster, G. M., and Oehler, L. T., "Vibration and Deflection of Rolled-Beam and Plate-Girder Bridges." HRB Bull. 124, 79 (1956).

5. Looney, C. T. G., "High-Speed Computer Applied to Bridge Impact." Journal of the Structural Division, Proc. ASCE, 84, Paper 1759 (Sept. 1958).
6. Scheffey, C. F., "Dynamic Load Analysis and Design of Highway Bridges." HRB Bull. 124, 16 (1956).
7. Edgerton, R. C., and Beecroft, G. W., "Dynamic Stresses in Continuous Plate-Girder Bridges." Transactions ASCE, 123:226 (1958).
8. Wen, R. K., "Dynamic Response of Beams Traversed by Two-Axle Loads." Jour. of the Engineering Mechanics Division, Proc. ASCE, Vol. 86: No. EM 5, p. 91 (Oct. 1960).
9. "Standard Plans for Highway Bridge Superstructure." Bureau of Public Roads, Washington, D. C. (1953).
10. "Tractor-Trailer Ride." Technical Board of Society of Automotive Engineers, New York (May 1956).
11. Wen, R. K., "Dynamic Behavior of Simple Span Highway Bridges Traversed by Two-axle Vehicles." Ph.D. Thesis, Univ. of Ill. (1957).
12. Oehler, L. T., "Vibration of Susceptibilities of Various Highway Bridge Types." Jour. of the Structural Division, Proc. ASCE, 83, Paper 1318 (July 1957).
13. Toledo-Leyva, J., and Veletsos, A. S., "Effects of Roadway Unevenness on Dynamic Response of Simple-Span Highway Bridges." Civil Engineering Studies, Structural Research Series No. 168, Univ. of Ill. (1958).

Appendix

NOTATIONS

AF = amplification factor
b = amplitude of sinusoidal unevenness on bridge surface
f_b = fundamental natural frequency of vibration of bridge, in cycles per sec
L = span length of bridge
m = number of half-sine waves along the bridge span
$q_b = y_o/y_s$ = dimensionless amplitude of initial bridge oscillation
q_p = dimensionless amplitude of initial pitching motion for vehicle, as defined by Eq. 11
q_v = dimensionless amplitude of initial vertical motion for vehicle, as defined by Eq. 10
s = spacing between axles
T_b = fundamental natural period of vibration of bridge
T_v = natural period of vibration of vehicle, idealized as a single-axle load
T_p = period of sinusoidal profile, defined by Eq. 13
t = time
v = vehicle speed
y_o = amplitude of initial bridge oscillation at midspan
y_s = maximum static deflection of bridge at midspan due to weight of vehicle
α = speed parameter, defined by Eq. 1
β_b = phase angle of initial bridge oscillation
β_p = phase angle of initial pitching motion of vehicle
β_v = phase angle of initial (vertical) bouncing motion of vehicle

Bridge Vibrations as Influenced by Elastomeric Bearings

WILLIAM ZUK, Professor of Civil Engineering, University of Virginia, and Highway Research Engineer, Virginia Council of Highway Investigation and Research

Inasmuch as many highway bridges are now being built with elastomeric bearings, it was considered desirable to study the vibration effects of such bridges. A theoretical analysis is presented, followed by several example calculations of short and medium span bridges.

General relationships are presented to determine the frequency of vibration of simple span bridges in the fundamental mode and the ratio of bridge beam deflections to the flexible bearing deflection under vibration subject to vehicular loads.

Contrasting the behavior of bridges with elastomeric bearings and with conventional rigid bearings, the following general conclusions are found: (a) the dynamic bridge deflections are increased; (b) the frequency of vibration is reduced (c) the elastomeric bearings add damping to the system; and (d) the dynamic stresses in the bridge are significantly reduced.

The fact that the impact stresses are reduced is quite revealing, as elastomeric bearings may lead to further structural economy, whereby less tolerance need be allowed for impact.

● MANY modern highway bridges are now being constructed in which the conventional rigid metal end bearings are being replaced by elastomeric bearing pads, such as neoprene. The primary purpose of using such neoprene bearings for short and medium span bridges is to reduce the cost of end bearing construction while still maintaining provision for expansion, contraction, and rotation of the bridge beams.

Because such supports are much more flexible than conventional supports, these elastomeric bearings will change the vibration characteristics of such bridges. The damping properties of elastomeric pads may also exert an influence on the vibration.

A completely rigorous theoretical study of bridge vibration including all the effects of oscillating moving loads, of the irregularities of road surface, of the infinite degree of freedom of the structure, and of the many manners of damping is a well-recognized task of monumental proportions. C. E. Inglis, in his book on vibrations, goes so far as to say, perhaps not too facetiously, that these "repulsive" mathematical equations are so complex that solutions cannot be had until after much prayer and fasting. As this study represents a first attempt to evaluate, in order of magnitude, the dynamic behavior of bridges supported on elastomeric bearings, the theoretical assumptions will be simplified to the ones believed to be the most influential on the behavior.

Several examples will be presented following the theory to indicate the trends of frequency, dynamic stresses, and deflections that would possibly occur under live loads.

THEORY

Undamped Frequency with Vehicular Load

The most critical bridge frequency is the one that is in resonance with the forcing frequency, as caused by a heavily loaded truck whose spring mass is oscillating vertically (1). For a simply supported bridge this critical frequency may be analytically obtained by placing the vehicle at the midspan and determining the fundamental mode caused by the bridge and truck masses.

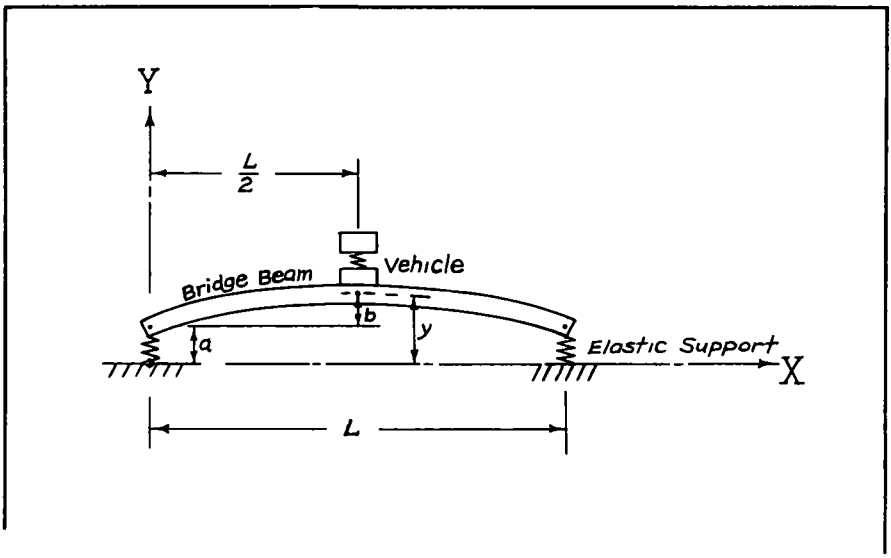

Figure 1. Vibration mode of bridge.

At resonance, the vertical oscillations of the vehicle will be in phase with the oscillations of the bridge itself. For simplicity of analysis, the oscillations of the vehicle will be assumed equal to that of the midspan of the bridge.*

Figure 1 shows the fundamental mode of vibration for a bridge beam supported on elastic bearings. Using Rayleigh's energy method of analysis (2), the total bridge deflection will be considered as

$$y = (a + b \sin \frac{\pi x}{L}) \cos pt = X \cos pt \qquad (1)$$

where p is the circular frequency, t is time, a is the maximum support deflection, and b is the maximum beam deflection.

In Rayleigh's method, the maximum potential energy, V, is equated to the maximum kinetic energy, T.

From Article 4 in Timoshenko (2)

$$V = \frac{EI}{2} \int_0^L \left(\frac{d^2 X}{dx^2}\right)^2 dx + 2 \frac{k}{2} a^2 \qquad (2)$$

where EI is the flexural rigidity of the beam, and k is the spring constant of the flexible support.

$$T = \frac{mp^2}{2} \int_0^L X^2 \, dx + \frac{1}{2} M v_i^2 \qquad (3)$$

where m is the mass of the bridge beam per unit length, M is the mass of the vehicle applied to the beam, and v_i is the maximum vertical velocity of the vehicle, taken as p(a + b) for harmonic motion.

After equating V to T and regrouping

---

*The approximation here lies in the possibility that the motion of the sprung mass of the vehicle may differ from that of the bridge, necessitating more involved analysis.

$$p^2 = \frac{EI\int_0^L \left(\frac{d^2X}{dx^2}\right)^2 dx + 2ka^2}{m\int_0^L X^2\,dx + M(a+b)^2} \tag{4}$$

This reduces to

$$p^2 = \frac{4\pi ka^2L^3 + \pi^5 EIb^2}{2\pi ma^2L^4 + 8abmL^4 + \pi mb^2L^4 + 2\pi Ma^2L^3 + 4\pi MabL^3 + 2\pi Mb^2L^3} \tag{5}$$

To obtain the fundamental mode, p is minimized by taking

$$\frac{\partial p^2}{\partial a} = 0 \quad \text{or} \quad \frac{\partial p^2}{\partial b} = 0.$$

Both expressions give the same results. After performing this operation and reducing, the support deflection, a, may be found in terms of the beam deflection, b, as follows:

$$a = nb \tag{6}$$

where

$$n = \pi^5 EI(Lm+M) - 2\pi KL^3(Lm+2M) + \left\{\left[2\pi KL^3(Lm+2M) - \pi^5 EI(Lm+M)\right]^2 + 16\pi^4 EIKL^3(2Lm+\pi M)^2\right\}^{1/2} \Big/ 8KL^3(2Lm+\pi M)$$

To obtain the circular frequency, p, Eq. 6 is substituted into Eq. 5. Both a and b will thereby be eliminated, and p may be determined as

$$p = \left[\frac{4\pi kn^2L^3 + \pi^5 EI}{2\pi mn^2L^4 + 8nmL^4 + \pi mL^4 + 2\pi Mn^2L^3 + 4\pi MnL^3 + 2\pi ML^3}\right]^{1/2} \tag{7}$$

The fundamental frequency in cycles per unit of time is therefore

$$f = \frac{p}{2\pi}$$

For comparative purposes, the fundamental frequency for a supported bridge beam with a load at the center (but with rigid bearings) may be found as outlined in Norris et al. (1, p. 423) and Timoshenko (2, pp. 26-27). By considering one-half the beam mass acting with the central load, the beam vibration problem may be resolved into a single degree of freedom problem whose frequency solution is

$$f' = \frac{1}{2\pi}\sqrt{\frac{k'}{mL/2 + M}} \tag{8}$$

where

$$k' = \frac{48EI}{L^3}$$

Amplitudes and Stresses with Damping

Without specific knowledge of the magnitude of the disturbing force, such as one caused by a moving truck, the exact amplitudes and stresses in a bridge cannot be determined. However, if one assumes that the same disturbing force acts on a bridge with flexible supports as with conventional rigid supports, a ratio of amplitudes between the two may be determined.

If one degree of freedom is assumed, a dynamic model of the loaded bridge with damped elastic bearings may be shown, as in Figure 2. C is the coefficient of viscous

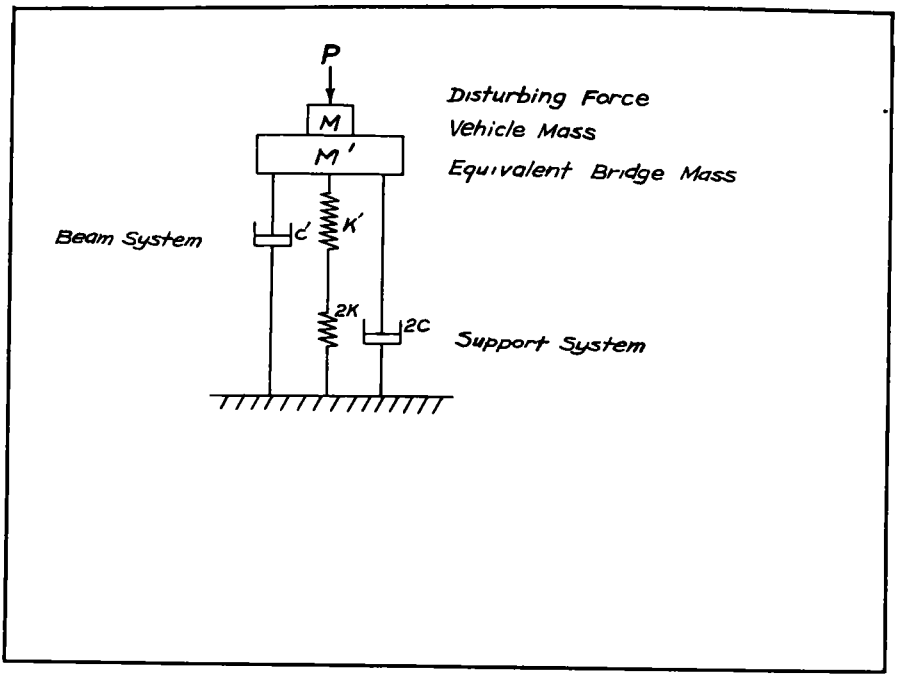

Figure 2. Dynamic model of loaded bridge.

damping for the elastic support and "C" is the coefficient of viscous damping for the beam itself.* If k is considered infinite and C considered zero, the model in Figure 2 then represents a bridge conventionally supported.

From Article 13 (2), the ratio of amplitudes for bridges with and without flexible supports for a resonance condition of forced vibration with damping may be obtained as follows:

$$\frac{\text{Amplit. elastic support}}{\text{Amplit. rigid support}} = R_A = \frac{C' f'}{C_e f} \tag{9}$$

where $C_e = C' + 2C$ = Effective damping of beam and support

$k_e = \frac{2k\,k'}{k' + 2k}$ = Effective spring constant of beam and support

Note that in Eq. 9 the bridge and vehicle masses divide out, as does the disturbing force, P. As will be shown later, this ratio, R_A, for dynamic deflections is generally greater than unity.

For comparative purposes, the ratio of live load nondynamic deflections with and without elastic supports for vehicles at crawl speed or stopped may be written as

$$R_A' = \frac{k'}{k_e} \tag{10}$$

This value of R_A' also exceeds unity.

*It is assumed that in conventionally supported bridges, the rollers or rockers are well lubricated, having negligible damping.

Since the maximum total dynamic bridge deflection consists of the support deflection, a, and the beam deflection, b, the increased bridge deflection obtained for elastically supported bridges from Eq. 9 does not necessarily imply increased dynamic flexural stresses.

If the dynamic amplitude for rigidly supported beams is taken as unity then R_A represents the dynamic amplitude for elastically supported beams. Therefore

$$a + b = R_A$$

However, using Eq. 6

$$b(1 + n) = R_A$$

Because the beam deflections are directly related to the dynamic flexural stress, S, the ratio of vibration induced stresses of bridges with and without elastic supports is given by

$$\frac{\text{Dyn. stress elastic support}}{\text{Dyn. stress rigid support}} = \frac{b}{1} = \frac{R_A}{1+n} = \frac{C'f'}{C_e f}\,\frac{1}{(1+n)} \qquad (11)$$

As will be shown later, this ratio, R_S is generally less than unity.

Again for comparative purposes, it is well to remember that no stress changes take place in the beam with vehicles at crawl speed or stopped (not considering vibration) for bridges with or without elastic supports. In simply supported beams, the beam stresses do not change under this "static" condition, because the stresses are independent of the end deflections.

EXAMPLES

Short Span Bridge

As an example of a short span highway bridge, a simply supported reinforced concrete structure, 36 ft in length is selected. H-20 loading is assumed, acting uniformly on five parallel stringers. The bearing pads are assumed made of neoprene, 1½ in. thick of 60 Durometer hardness. Based on compressive load-deflection curves by Biggs and Suer (3), the equivalent spring constant, k, for this particular pad is 32×10^4 lb per in. From Yerzley Oscillograph readings performed in accordance with test method ASTM D 945 as supplied by the E. I. DuPont de Nemours and Co. the coefficient of viscous damping, C, is computed as 3.11 lb-sec per in.*

Other pertinent data for this bridge are as follows:

Mass per unit length of beam = m = 0.282 lb-sec^2 per in.
Mass of vehicle per beam = M = 21.7 lb-sec^2 per in.
Modulus of elasticity of beam = E = 3×10^6 lb per sq in.
Moment of inertia of beam = I = 73×10^3 in.^{4}

The coefficient of viscous damping, C, of the bridge beam itself is difficult to pinpoint, as many accumulated minor factors are involved. A number of citations to experimental damping coefficients are given by DuPont de Nemours and Co. (4), Foster and Oehler (5) and Inglis (6). A decision of judgment therefore had to be made in the selection of the coefficient, C, based on the significant structural similarities between the example bridge and the bridge in the previously cited references. For this bridge the value of C = 460 lb-sec per in. is taken as a representative mean.

By means of Eq. 6, the relationship is found that

$$a = 0.597\, b$$

*This constant was also checked by an independent method by the author.

By use of Eq. 7, the fundamental frequency is found as

$$f = 6.5 \text{ cps}$$

By means of Eq. 9, the ratio of dynamic amplitude, R_A, with and without elastic support is

$$R_A = 1.44$$

By means of Eq. 11, the ratio of dynamic stresses, R_S, with and without elastic support is

$$R_S = 0.90$$

For comparative purposes, the bridge frequency with rigid supports is computed from Eq. 8 as

$$f' = 9.5 \text{ cps}$$

Also for comparative purposes, the ratio of nondynamic live-load deflection with and without elastic supports is computed from Eq. 10 as

$$R_A' = 1.45$$

Thus to summarize this example of a short span bridge, the consequences of using elastic bearings instead of conventional bearings are the following:

1. Reduction of the frequency of vibration by a ratio $R_f = 0.685$. This reduction in frequency may have significant consequences if the frequency is reduced below 6.5 cps as tests by Foster and Oehler (5) indicate this to be the threshold of pedestrian distress. If the frequency is reduced below 3 cps, undesirable resonance between vehicles and structure may result.
2. Increase of the total dynamic amplitude by a ratio $R_A = 1.44$ of which 37.5 percent of the total amplitude lies in the support pads. However, this increased amplitude is not serious within itself.
3. Increase of the over-all damping by a ratio $R_d = 1.01$. This change is negligibly small.
4. Decrease of the dynamic beam stresses by a ratio $R_S = 0.90$. This decrease is significant as less allowance may perhaps be permissible for impact stresses.
5. Increase of the nondynamic live-load deflection by a ratio $R_A' = 1.45$ of which 31 percent of the total deflection lies in the bearings.
6. Absence of change in the nondynamic live-load or dead-load beam stresses; i.e., $R_S' = 1$.

Medium Span Bridge

A 78-ft simply supported bridge with prestressed concrete beams is taken as another example. H-20 loading is again assumed. The bearing pads are assumed to be the same as in the prior example. The data pertinent to this bridge are given as follows:

$m = 0.286$ lb-sec^2 per in.
$M = 27.7$ lb-sec^2 per in.
$E = 5 \times 10^6$ lb per sq in.
$I = 640.57 \times 10^3$ in.
$k = 32 \times 10^4$ lb per in.
$C = 3.11$ lb-sec per in.
$C' = 866$ lb-sec per in.

From Eq. 6	a	$= 0.4077\ b$
From Eq. 7	f	$= 4.49$
From Eq. 9	R_A	$= 1.20$
From Eq. 11	R_S	$= 0.85$
From Eq. 8	f'	$= 5.42$ cps
From Eq. 10	R_A'	$= 1.29$

Summarizing the results of this example, it is seen that the use of elastic bearings in place of rigid bearings achieves the following:

1. Reduction of the frequency of vibration by a ratio $R_f = 0.83$ putting the bridge in a more critical low frequency range.
2. Increase of the total dynamic amplitude by a ratio $R_A = 1.20$, in which 29 percent of the total amplitude lies in the flexible bearings.
3. Increase of the over-all damping by ratio $R_d = 1.01$.
4. Decrease of the dynamic beam stresses by a ratio $R_S = 0.85$.
5. Increase of the nondynamic live-load deflection by a ratio $R_A' = 1.29$, of which 22.5 percent of the total deflection lies in the bearings.
6. Absence of change in the nondynamic live-load or dead-load beam stresses, making $R_S' = 1$.

To illustrate the effects of thicker bearing pads, consider the same 78-ft bridge but with 3-in. thick neoprene pads of Durometer hardness 70. For this pad $k = 23.3 \times 10^4$ lb per in. and $C = 5.19$ lb-sec per in.

Then from Eq. 6	$a = 0.542b$
From Eq. 7	$f = 4.42$ cps
From Eq. 9	$R_A = 1.21$
From Eq. 11	$R_S = 0.79$
From Eq. 8	$f' = 5.42$ cps
From Eq. 10	$R_A' = 1.40$

Thus, the consequences of using thick elastic bearings in place of conventional rigid bearings are the following:

1. Reduction of the frequency of vibration by a ratio $R_f = 0.81$.
2. Increase of the total dynamic amplitude by a ratio $R_A = 1.21$, in which 35 percent of the total amplitude lies in the supports.
3. Increase of the over-all damping by a ratio $R_d = 1.01$.
4. Decrease of the dynamic beam stresses by a ratio $R_S = 0.79$.
5. Increase of the nondynamic live-load deflection by a ratio $R_A' = 1.40$, of which 28.5 percent of the total deflection lies in the bearings.
6. Absence of change in the nondynamic live-load or dead-load beam stress.

A comparative study of the dynamic effects of the same bridge with thick and thin bearing pad shows that impact stresses are reduced an additional 6 percent for thick pads, or a total of 21 percent over rigid bearings.

CONCLUSIONS

Despite the fact that the example bridges are of different types and lengths, the general trends of amplitudes, stresses, and frequencies are similar.

Flexible supports will decrease the natural bridge frequency; however, the example problems indicate the reduction in the order of magnitude of 20 to 30 percent, being larger for shorter spans. Bridges normally stiff enough with rigid bearings may therefore become undesirably flexible with elastomeric bearings, especially if frequencies are in the range of 4 to 6 cps.

It is also obvious that elastic supports will increase both dynamic and nondynamic amplitudes and deflections. However, the examples show that the increase is slightly less for dynamic than for nondynamic live-loads.

The small amount of damping added to the system by the elastomeric supports is negligibly small, and even this increase is questionable inasmuch as the theoretical assumption is made that the conventional supports have no damping.

In cases of rusty or dirty conventional supports that have an appreciable amount of friction damping, a replacement with elastomeric bearings may actually decrease the total damping.

The most interesting and somewhat paradoxical conclusion to be drawn from this study however, is that the dynamic beam stresses actually decrease by about 15 percent, despite an increase in total deflection of about 30 percent. The explanation lies

in the fact that the total deflection is due to the sum of the support and beam deflections; whereas the stresses are due only to the beam deflection portion of the total deflection. The explanation may also be stated in another manner, namely, the total impact energy is distributed to both the beam and the elastic support. Because the supports absorb a portion of this energy, there is less energy for the beam to absorb. In a general way, the elastic supports act as shock absorbers.

The examples show that the thicker bearing pads tend to reduce impact stresses materially as compared to thinner pads. Thus, the question of design arises if perhaps designing for thicker pads is not to be preferred to reduce impact stresses, providing that frequency levels are not critical. A lower impact stress would certainly be advantageous in many respects, including that of improving a bridge's fatigue life.

Unfortunately, immediate experimental verification to the theoretical conclusions is not available. Until it is, certain caution is suggested in adopting the theoretical conclusions for design use, as the theory is based on many simplifying assumptions.

Relatively easy laboratory experiments would generally be useless due to the virtual impossibility of scaling and reproducing vehicular dynamics, deck roughness, and damping. Field tests would therefore provide the only reliable confirmation for design use. In field testing, two possibilities appear feasible. The first is to design twin bridges (as on a dual highway) one with conventional bearings and the other with elastomeric bearings. Instrumenting both bridges would then provide comparative information. However, variations in deck roughness between the two bridges may conceivably be a significant factor in impact. Therefore, a second alternate for field testing would be to use but one bridge but designed for interchanging rigid bearings and elastic bearings. The second alternate is more costly, although more precise. The Bridge Division of the Virginia Department of Highways is currently considering erecting such bridges from which reliable data may be found. It is hoped that this may be done in the near future.

ACKNOWLEDGMENTS

This study was made under the auspices of the Virginia Council of Highway Investigation and Research, under the direction of Mr. Tilton E. Shelburne, in cooperation with the University of Virginia. Special acknowledgment is also made to Mr. Paxson and his bridge committee of the Highway Research Board for their enlightening comments and suggestions concerning this subject.

REFERENCES

1. Norris, Hanson, Holley, Biggs, Namyet, and Minami, "Structural Design for Dynamic Loads." McGraw-Hill, New York (1959).
2. Timoshenko, "Vibration Problems in Engineering." 3rd ed., Van Nostrand, New York (1955).
3. "Design of Neoprene Bridge Bearing Pads." E.I. DuPont de Nemours and Co.
4. Biggs, J.M., and Suer, H.S., "Vibration Measurements on Simple-Span Bridges." HRB Bull. 124, 1-15 (1956).
5. Foster, G.M., and Oehler, L.T., "Vibration and Deflection of Rolled-Beam and Plate-Girder Bridges." HRB Bull. 124, 79-110 (1956).
6. Inglis, C. E., "A Mathematical Treatise on Vibrations in Railway Bridges." Cambridge, Teddington Univ. Press, (1934).

Truss Deflections by Electronic Computation of The Williot-Mohr Diagram

ZA LEE MOH, Structural Designer, and CHARLES E. COOPER, Junior Engineer, State Highway Department of Indiana, Indianapolis

This paper describes the method and procedure used in a digital computer program to find horizontal and vertical movements of all joints of a truss, given the member stresses and the structure properties. The method presented is a solution by analytic geometry of the well-known graphical method of Williot and Mohr. The discussion of the basic program procedure is accompanied by a simplified flow chart. A sample case is included to illustrate the speed, accuracy, and flexibility of the program.

●THE ADVANTAGES of truss construction are well known, as witnessed by its widespread use in bridge building. A major disadvantage, however, has been that the design calculations are usually very time-consuming, particularly for indeterminate trusses. This disadvantage, however, is becoming less and less significant with the growing use of the digital computer. There have already been several programs developed for stress analysis of determinate and indeterminate trusses. The program described in this paper deals with another important phase—that of deflections. The necessity for truss deflection computations arises both in the design office, as in the determination of secondary stresses, and in the field, as in the erection of continuous trusses by the cantilever method.

Representative of the several procedures for determining truss deflections are the virtual work, the elastic weight, and Williot-Mohr diagram methods. The method of virtual work is perhaps the best and most direct method for computing one component of deflection for one joint, but this process becomes quite lengthy if the true absolute deflections of all joints are needed. The elastic weight method comes a step closer, but even it is limited to only one component for each joint. This method also becomes lengthy if both the horizontal and vertical components are to be computed. The Williot-Mohr diagram yields the resultant deflections of all joints by a single solution. As a graphical method, it too has its disadvantages. Although it is theoretically sound, it is by its very nature limited in accuracy, and for very large structures, it becomes particularly troublesome in matters of scaling and orientation on the paper. But these disadvantages are easily overcome by an algebraic procedure that corresponds to the graphical one. The computations involved in the solution by analytic geometry of the Williot-Mohr diagram are quite simple and are highly repetitive in nature, thus making this method well suited to the electronic computer. The analytic solution is both accurate and fast. It is the purpose of this paper to describe an electronic computer program and the method used therein for the computation of truss deflections.

NOTATION

Specific symbols are defined where they appear in this paper. In general, however, the following rules apply:

1. Superscripts T, W, and M refer, respectively, to the truss diagram, the Williot diagram, and the Mohr correction diagram.
2. Subscripts refer to specific points or vectors. X and Y subscripts are used to denote, respectively, x and y components of vectors.

3. Points on the different diagrams are designated by an upper case letter with a superscript. Thus, for example, A^W is the point on the Williot diagram that corresponds with point (or joint) A^T of the truss diagram.

4. The relative positions or locations of the various points are defined by x and y coordinates. For example, (x_A^W, y_A^W) are the coordinates of point A^W on the Williot diagram.

THE WILLIOT-MOHR METHOD

Though no attempt is made here to develop or prove the Williot-Mohr method for determining truss deflections, the following graphical procedure is described as a basis for the development of the analytic procedure.

The Williot diagram, which is drawn first, gives the movements of all joints of the truss with respect to one of the joints and a member that enters that joint. If the member that was used as a direction reference actually rotates with the deformation of the truss, the Mohr correction diagram must be added to give the true absolute movements of all the joints. The scaling of the Mohr correction diagram depends on the amount that the original reference member actually rotates, and the positioning of the correction diagram depends on the actual movement of the original reference joint. If a truss joint that is actually fixed against translation is used as the reference point for the Williot diagram, then both the Williot diagram deflection and the Mohr diagram correction for that joint would be zero. A second point on the Williot diagram may be located by using one of the members entering the fixed joint as a direction reference. A vector equal to the deformation of that member is drawn from the reference point in the direction in which the opposite joint of that member moves with respect to the fixed joint. The location of the first two points on the Williot diagram is shown in Figure 1. Point F^W on the Williot diagram corresponds to the fixed joint F^T on the truss diagram. The member connecting joints F^T and H^T is used as a direction reference for the Williot diagram. The vector $\overrightarrow{F^WH^W}$ represents the magnitude and direction of the movement of joint H^T with respect to joint F^T, and thereby the position of point H^W on the Williot diagram is established. Note that $\overline{F^WH^W}$ is drawn parallel to $\overline{F^TH^T}$.

After having established the first two points, the Williot diagram is completed by proceeding from joint to joint in a series of similar steps. In each step two known Williot diagram points and the deformations of two members are used to establish the position of a third Williot diagram point. One such step is shown in Figure 2, which shows a typical triangular truss panel (Fig. 2a) with joints A^T, B^T, and C^T and the corresponding portion of the Williot diagram (Fig. 2b). Points A^W and B^W are the known Williot diagram points and C^W is the point to be determined. The location of point C^W is determined as follows:

1. The intermediate point W_{AC} is established by the vector A^WW_{AC} which is

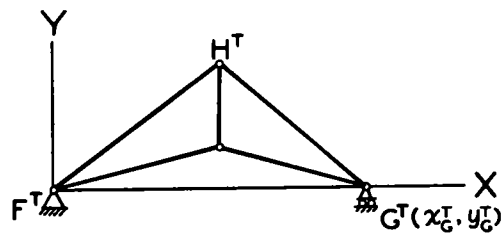

(a) TRUSS DIAGRAM

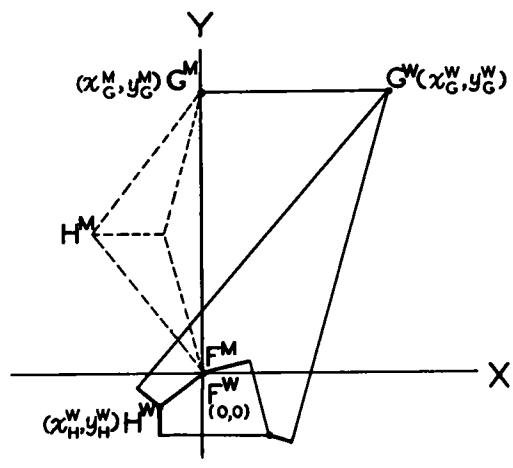

(b) WILLIOT-MOHR DIAGRAM

Figure 1. Example truss and Williot-Mohr diagrams.

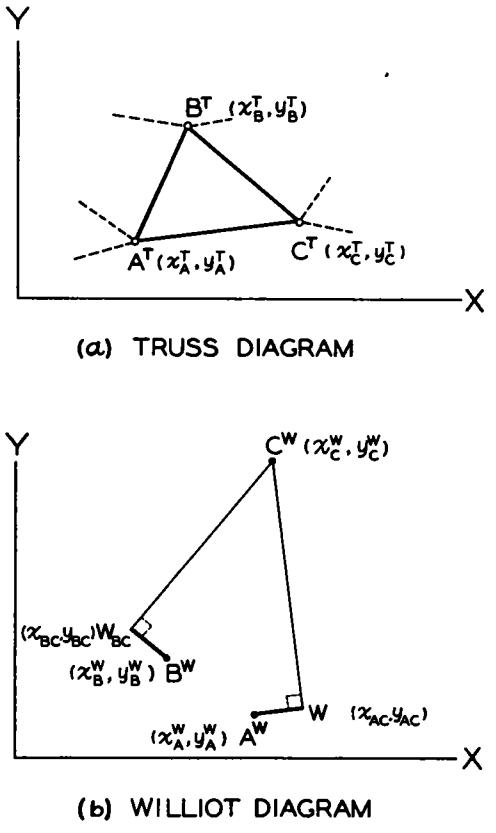

Figure 2. Typical triangular truss panel with corresponding portion of Williot diagram.

proportional in length to the deformation of member AC and is drawn parallel to that member from A^W to W_{AC} in the direction that C moves with respect to A^T. The intermediate point W is established in like manner with respect to member BC.

2. Perpendiculars are erected at points W_{AC} and W_{BC} and are extended until they intersect to locate C^W.

This procedure is repeated until a corresponding Williot diagram point has been established for each joint of the truss.

With the Williot diagram completed, the Mohr correction diagram can be drawn to give the true absolute movements of all the joints. Because the fixed joint of the truss was used as the starting point for the Williot diagram, the correction involves only the rotation of the structure about that joint until the guided joint is brought back into its predetermined path. The Mohr diagram is geometrically similar to the truss configuration, and furthermore, the lines of the Mohr diagram are perpendicular to the corresponding lines of the truss diagram. Referring again to Figure 1, F^M coincides with F^W because F^T is actually fixed in position. Another Mohr diagram point, G^M, is defined by the intersection of a line drawn through G^W parallel to the direction of movement of the guided joint G^T and the line drawn through F^W perpendicular to the line connecting points F^T and G^T. With these two points, F^M and G^M, determined, the rest of the Mohr diagram can be filled in to scale in accordance with the preceding.

THE ANALYTIC PROCEDURE

Input Data

The information needed for the construction of the Williot-Mohr diagram consists of an adequate description of the truss configuration and the deformation (shortening or lengthening) of each member. For the computer program the truss is described by means of two tabulations. The first is a tabulation of joints by number giving a pair of of rectangular coordinates for each joint. The second is a tabulation of members giving the joint numbers of the two joints that each member enters. The coordinates axes are positioned on the truss diagram so that the entire truss lies in the first quadrant, thus eliminating negative coordinates.

In addition to the joint and member tabulations, the numbers of the fixed and guided joints and the direction in which the guided joint moves must be indicated. The direction of movement of the guided joint is expressed as an angle, β', measured from the X-axis. Also, because the output deflections (answers) are to be given in x and y components, the desired directions for these components (such as horizontal and vertical) are indicated by an angle, α, measured from the respective coordinate axes used to describe the truss. For both α and β' the usual sign convention applies; i.e., counterclockwise is positive, clockwise is negative. Note that, regarding algebraic sign, these angles are given with respect to the original coordinate axes used to describe the truss configuration.

The data needed for computing the member deformations include the axial force, cross-sectional area, and length of each member along with the modulus of elasticity of the truss material. The axial forces (stresses), S, and the cross-sectional areas, A, are included in the member table, and the lengths are determined from the joint coordinates. The appropriate conversion factors may be incorporated into the figure for modulus of elasticity in order that all other data may be entered "as found" without regard to units. Based on the data thus provided, the computations for truss deflections can be started.

Preliminary Computations

The guiding principle in the preparation of the format for input data was that these data should be limited as nearly as possible to those quantities that are readily available, leaving conversions and other preliminary computations to the computer program. The first of these preliminary computations to be considered here is that for member deformations. Because the subsequent computations will involve only x and y components, the unit deformation rather than the total deformation is computed for each member at this time. Unit deformation, δ, may be defined as the amount by which a unit length of a member elongates or shortens. In accordance with the definition of modulus of elasticity,

$$\delta = \frac{S}{A\ E} \tag{1}$$

The algebraic sign, of course, depends on the sign of S, which is considered positive for tension and negative for compression.

Having oriented the original coordinate axes on the basis of convenience for describing the truss configuration, the next step is to transform the coordinates so that (a) the origin coincides with the fixed joint and (b) the X and Y axes lie, respectively, in the directions in which the final deflection components are desired; e.g., horizontal and vertical. The formulas for transformation of coordinates are

$$x = (y' - k)\sin\alpha + (x' - h)\cos\alpha \tag{2a}$$

$$y = (y' - k)\cos\alpha - (x' - h)\sin\alpha \tag{2b}$$

in which x and y are the coordinates of a point in the new system, x' and y' are the coordinates of the same point in the old system, h and k are the coordinates of the origin of the new system in terms of the old system, and α is the angle that the new axes makes with the corresponding old axes.

Figure 3a shows a sample truss diagram with angles α and β' labeled and the original coordinate axes used to describe the truss. Figure 3b shows the positioning of the new axes, presuming that in this case horizontal and vertical components of joint deflections are desired. Note that the angle β is found as follows:

$$\beta = \beta' - \alpha \tag{2c}$$

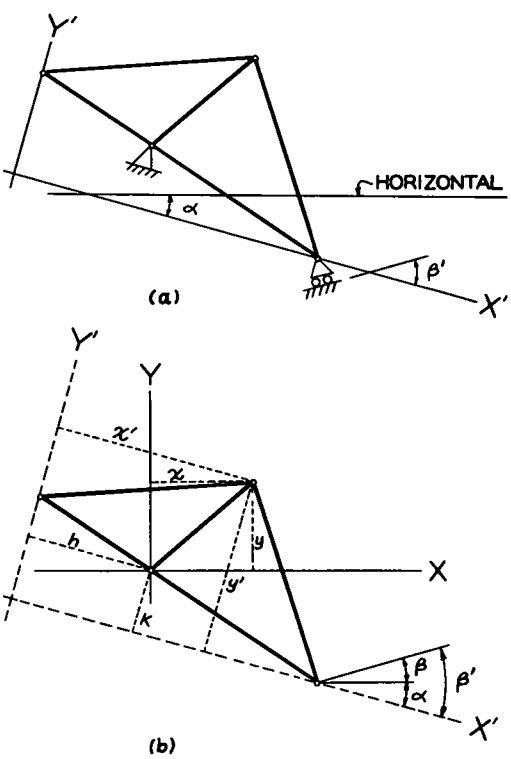

Figure 3. Orientation of coordinate axes.

The Analytic Solution

Once the unit deformations have been computed and the coordinate axes properly

oriented as indicated above, the rest of the procedure involves only x and y components. As in the graphical solution, the first two points to be located on the Williot diagram are those corresponding with the fixed joint and the opposite joint of a member that enters the fixed joint. The Williot diagram coordinates (x_F^W , y_F^W)of the point, F^W, which corresponds with the fixed joint, F^T, are both equal to zero (see Fig. 1). If the member, FH, which connects joints F^T and H^T, is used as the direction reference for the Williot diagram, then the Williot diagram coordinates for point H^W are computed by resolving the movement of joint H^T with respect to joint F^T into x and y components. Thus:

$$x_H^W = (x_H^T - x_F^T)\,\delta_{FH}$$

$$y_H^W = (y_H^T - y_F^T)\,\delta_{FH}$$

in which δ_{FH} is the unit deformation for the member FH. But because the truss diagram coordinates for the fixed joint are zero, the equations become

$$x_H^W = x_H^T \delta_{FH} \tag{3a}$$

$$y_H^W = y_H^T \delta_{FH} \tag{3b}$$

The remaining step-by-step procedure for completing the table of Williot diagram coordinates is again analogous to that of the graphical procedure. However, instead of using the length of a member to compute its deformation, the x and y components of the vector representing the distance from the near end of the member to the far end must be used in order to account for the direction in which the far end moves with respect to the near end. If joints A^T and B^T are at the "near ends" of members AC and BC, respectively, and if the "far ends" of both members enter joint C^T (see Fig. 2a), then the length vectors are computed as follows:

$$L_{XA} = x_C^T - x_A^T \tag{4a}$$

$$L_{YA} = y_C^T - y_A^T \tag{4b}$$

$$L_{XB} = x_C^T - x_B^T \tag{4c}$$

$$L_{YB} = y_C^T - y_B^T \tag{4d}$$

in which L_{XA} is the x component of the vector $\overrightarrow{A^T C^T}$, L_{YA} is the y component of the same vector, etc. For the typical triangular truss panel of Figure 2, the Williot diagram coordinates of points A^W and B^W are known and the coordinates of point C^W are to be computed. The intermediate points W_{AC} and W_{BC} are obtained by adding the respective vectors representing the movement of joint C^T with respect to joint A^T parallel to member AC and the movement of joint C^T with respect to joint B^T parallel to member BC to the points A^W and B^W. Therefore, the coordinates of these intermediate points may be computed by using the following equations:

$$x_{AC} = L_{XA}\delta_{AC} - x_A^W \tag{5a}$$

$$y_{AC} = L_{YA}\delta_{AC} - y_A^W \tag{5b}$$

$$x_{BC} = L_{XB}\delta_{BC} - x_B^W \tag{5c}$$

$$y_{BC} = L_{YB}\delta_{BC} - y_B^W \tag{5d}$$

Finally, the location of point C^W is defined by the intersection of the lines perpendicular to the vectors $A^W W_{AC}$ and $B^W W_{BC}$ and passing through points W_{AC} and W_{BC}, respectively. The general equation of a line given a point (x_1, y_1) on that line and the slope, m, of a line normal to it is

$$y = y_1 - \frac{1}{m}(x - x_1)$$

The slopes of vectors $\overrightarrow{A^W W_{AC}}$ and $\overrightarrow{B^W W_{BC}}$ are equal to $\frac{L_{YA}}{L_{XA}}$ and $\frac{L_{YB}}{L_{XB}}$, respectively. By substituting these slopes and the coordinates of the corresponding points W_{AC} and W_{BC} into the general equation above, the following equations for the lines $\overline{W_{AC}C^W}$ and $\overline{W_{BC}C^W}$ result:

$$y = y_{AC} - \frac{L_{XA}}{L_{YA}}(x - x_{AC})$$

$$y = y_{BC} - \frac{L_{XB}}{L_{YB}}(x - x_{BC})$$

Solving these two equations simultaneously for the coordinates, (x_C^W, y_C^W), of point C^W yields

$$x_C^W = \frac{\frac{x_{AC}L_{XA}}{L_{YA}} - \frac{x_{BC}L_{XB}}{L_{YB}} + y_{AC} - y_{BC}}{\frac{L_{XA}}{L_{YA}} - \frac{L_{XB}}{L_{YB}}} \tag{6a}$$

$$y_C^W = \frac{\frac{y_{AC}L_{YA}}{L_{XA}} - \frac{y_{BC}L_{YB}}{L_{XB}} + x_{AC} - x_{BC}}{\frac{L_{YA}}{L_{XA}} - \frac{L_{YB}}{L_{XB}}} \tag{6b}$$

Therefore, Eqs. 4-6 may be used to locate each successive Williot diagram point with respect to the coordinate axes after the two starting points have been located, the first being at the origin and the second by Eqs. 3a and 3b. Special consideration must be given, however, if the result of any one of the Eqs. 4a-4d is zero, as would be the case for a member parallel to either coordinate axis. The following rules apply:

$$\text{If } L_{XA} = 0; \text{ then } y_C = y_{AC} \tag{7a}$$

$$\text{If } L_{YA} = 0; \text{ then } x_C = x_{AC} \tag{7b}$$

$$\text{If } L_{XB} = 0; \text{ then } y_C = y_{BC} \tag{7c}$$

$$\text{If } L_{YB} = 0; \text{ then } x_C = x_{BC} \tag{7d}$$

Having completed the Williot diagram as indicated above, the next step is to compute the angle, θ, through which the truss must be rotated about its fixed joint to bring the guided joint back into its previously designated path. Because θ is quite small in any practical case, it may be taken as equal to its tangent, thus:

$$\theta = \frac{y_G^W - x_G^W \tan\beta}{x_G^T} \tag{8}$$

in which x_G^T is the x coordinate of the guided joint (truss diagram) and (x_G^W, y_G^W) are the coordinates of the corresponding Williot diagram point. The coordinates for each point on the Mohr correction diagram (see Fig. 1b) may be computed by the following equations:

$$x_N^M = -\theta\, y_N^T$$

$$y_N^M = \theta\, x_N^T$$

in which x_N^T and y_N^T are the coordinates of any joint, N^T, of the truss diagram and x_N^M and y_N^M are the coordinates of the corresponding Mohr correction diagram point.

The x and y components of the true absolute movement of each truss joint may be obtained by subtracting, respectively, the coordinates of the Mohr diagram points from the coordinates of the corresponding Williot diagram points; thus:

$$D_{XN} = x_N^W + \theta\, y_N^T \tag{9a}$$

$$D_{YN} = y_N^W - \theta\, x_N^T \tag{9b}$$

in which D_{XN} and D_{YN} are the x and y components of the deflection of any joint, N^T, respectively.

THE COMPUTER PROGRAM

A computer program for the computation of truss deflections based on the described method was written for the IBM 650 data processing system. This program follows basically the procedure set forth in the simplified flow chart, Figure 4. The program was limited arbitrarily to trusses with up to 99 non-redundant members. It is, of course, also limited to those truss deflection problems that can be solved by the Williot-Mohr method.

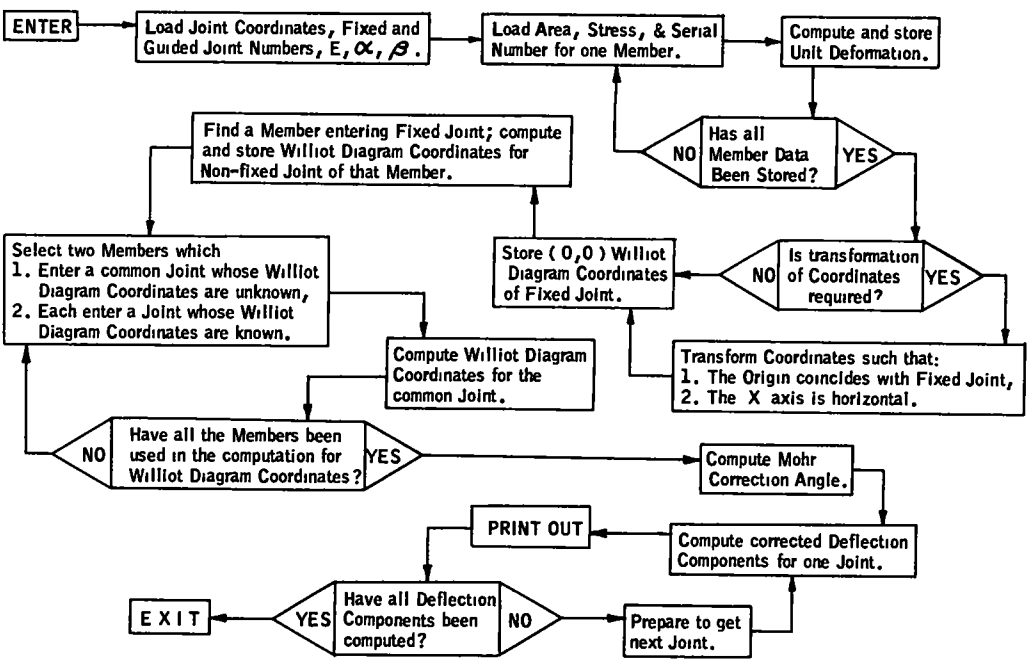

Figure 4. Simplified flow chart for computer program.

Input data include the joint and member tabulations, the modulus of elasticity, and the respective numbers of the fixed and guided joints, as previously indicated. In addition to these, the joint and member counts are required. The output consists of the x and y components of deflection for each joint.

Running time varies from about 4 to 12 sec per joint depending on the order in which the truss members are numbered. If the members are numbered in the order in which they would be used in the construction of the Williot diagram, the searching time for the machine is greatly reduced. Regardless of member numbering, however, the total running time for a 99-member truss would not exceed about 10 min.

SAMPLE CASE

The New Albany-Louisville Bridge on Interstate 64 over the Ohio River was used to illustrate the described truss deflection program. The bridge is a double-decked, tied-arch truss 797.5 ft long from fixed joint to guided joint. Bridge elevations and joint coordinates are shown in Figure 5. Physical properties and dead-load stresses are listed in Table 1. Using for the modulus of elasticity of the truss material 29,000 ksi, the horizontal and vertical components of deflection (Table 2) were computed for each joint in a total of 3 min 5 sec, including read-in and punch-out time, by the IBM 650 digital computer.

TABLE 1

PHYSICAL PROPERTIES AND DEAD LOAD STRESSES[a]

Member Serial Number			Area	Stress
Member No.	From Joint	To Joint	(sq in.)	(kips)
01	01	02	142.00	-710
02	01	03	227.40	-5517
03	02	03	45.20	737
04	02	04	79.10	-474
05	03	04	70.80	-749
06	04	05	45.20	782
07	03	05	202.60	-4821
08	05	06	54.70	-726
09	04	06	96.70	-1095
10	06	07	40.40	711
11	05	07	175.50	-4031
12	07	08	50.00	-572
13	06	08	131.80	-1751
14	08	09	38.20	638
15	07	09	151.80	-3284
16	09	10	39.60	-375
17	08	10	120.40	-2342
18	10	11	36.30	601
19	09	11	130.10	-2620
20	11	12	37.70	-310
21	10	12	130.70	-2838
22	12	13	34.40	563
23	11	13	118.80	-2029
24	13	14	35.20	-182
25	12	14	148.70	-3293
26	14	15	32.60	486
27	13	15	132.20	-1496
28	15	16	33.80	-118
29	14	16	161.00	-3665
30	16	17	32.60	435
31	15	17	101.30	-1056

TABLE 1 (Continued)

PHYSICAL PROPERTIES AND DEAD LOAD STRESSES[a]

Member Serial Number			Area	Stress
Member No.	From Joint	To Joint	(sq in.)	(kips)
32	17	18	33.80	3
33	16	18	171.80	-3991
34	18	19	34.40	309
35	17	19	101.30	-676
36	19	20	31.10	85
37	18	20	175.50	-4208
38	20	21	39.70	231
39	19	21	83.80	-418
40	21	22	31.10	214
41	20	22	179.50	-4368
42	22	23	42.30	39
43	21	23	75.00	-228
44	23	24	26.70	240
TIE	01	46	132.00	4582

[a]Structure is symmetrical about member 44.

TABLE 2

OUTPUT DEFLECTIONS: HORIZONTAL AND VERTICAL COMPONENTS

Joint No.	Horiz. Comp. (ft)	Vert. Comp. (ft)	Joint No.	Horiz. Comp. (ft)	Vert. Comp. (ft)
01	0.000	0.000	24	0.478	1.779
02	0.245	0.012	25	0.448	1.749
03	0.080	0.185	26	0.475	1.756
04	0.287	0.205	27	0.424	1.672
05	0.161	0.386	28	0.476	1.675
06	0.338	0.407	29	0.409	1.556
07	0.238	0.596	30	0.487	1.556
08	0.401	0.612	31	0.409	1.404
09	0.307	0.809	32	0.508	1.400
10	0.460	0.821	33	0.422	1.227
11	0.365	1.019	34	0.544	1.221
12	0.504	1.030	35	0.452	1.030
13	0.411	1.221	36	0.591	1.019
14	0.533	1.227	37	0.496	0.821
15	0.447	1.400	38	0.649	0.809
16	0.547	1.404	39	0.554	0.612
17	0.469	1.556	40	0.718	0.596
18	0.546	1.556	41	0.618	0.407
19	0.479	1.675	42	0.794	0.386
20	0.532	1.672	43	0.669	0.205
21	0.481	1.756	44	0.876	0.185
22	0.508	1.749	45	0.710	0.012
23	0.478	1.788	46	0.956	0.000

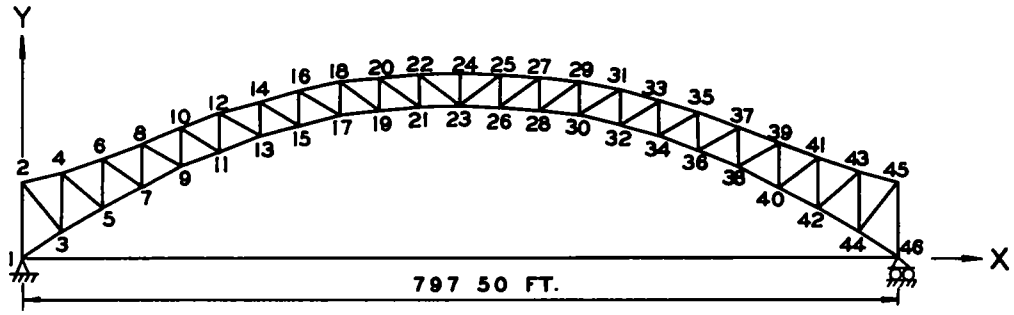

JT.NO	X	Y	JT.NO	X	Y	JT.NO.	X	Y	JT.NO	X	Y	JT.NO.	X	Y
02	0.00	70.00	11	181.25	98.35	20	326.25	166.00	29	507.50	161.00	38	652.50	83.31
03	36.25	24.30	12	181.25	134.00	21	362.50	138.84	30	507.50	129.59	39	688.75	106.00
04	36.25	69.33	13	217.50	111.07	22	362.50	169.00	31	543.75	154.00	40	688.75	65.95
05	72.50	46.28	14	217.50	145.00	23	398.75	140.00	32	543.75	121.49	41	725.00	91.33
06	72.50	91.33	15	253.75	121.49	24	398.75	170.00	33	580.00	145.00	42	725.00	46.28
07	108.75	65.95	16	253.75	154.00	25	435.00	169.00	34	580.00	111.07	43	761.25	79.33
08	108.75	106.00	17	290.00	129.59	26	435.00	138.84	35	616.25	134.00	44	761.25	24.30
09	145.00	83.31	18	290.00	161.00	27	471.25	166.00	36	616.25	98.35	45	797.50	70.00
10	145.00	121.00	19	326.25	135.37	28	471.25	135.37	37	652.50	121.00	46	797.50	0.00

NEW ALBANY-LOUISVILLE BRIDGE

Figure 5. Sample case (New Albany-Louisville Bridge).

REMARKS

The method just described for the analysis of truss deflection is nothing new. It is only an analytic version of the commonly used Williot-Mohr diagram. The procedure is also similar in many respects to K. H. Chu's method (1), which was developed for use with a desk calculator. The sign convention is always troublesome in the Williot-Mohr graphical method, but it is taken care of automatically by the computer program. Length of each member is determined from the joint coordinates, a fact that also simplifies the input data.

ACKNOWLEDGMENT

The authors wish to express their sincere thanks to C. R. Ruminer and M. G. Dukes, both of the State Highway Department of Indiana, for their encouragement and guidance.

REFERENCE

1. Chu, K. H., "Truss Deflections by the Coordinate Method." Trans. ASCE, 117: 317-336 (1952).

Fatigue in Welded Beams and Girders

W. H. MUNSE and J. E. STALLMEYER, Professors of Civil Engineering,
Department of Civil Engineering, University of Illinois, Urbana

● IN RECENT YEARS there has been a marked increase in the use of welding of highway bridges, particularly for welded girder bridges. At the same time, this increase in the application of welding to bridges has resulted in a greater need for information concerning the fatigue behavior of such structures.

The current AWS design specifications (1) for welded bridges are based on a consideration of fatigue. The problem of designing for fatigue, however, is complicated by the fact that the fatigue behavior varies considerably for the component members, connections, and details of such structures. Some members or details may receive relatively few and others may receive many applications of maximum load, some members or locations may be subjected to relatively small changes in stress and others may receive reversals or large ranges of stress during a loading. These are factors of major importance and need to be taken into account in design if the structures are to resist efficiently and economically the loads to which they are subjected.

Also of importance to the behavior of structures subjected to repeated loads is the geometry of the details of the individual parts that make up the structure. The resulting stress concentrations have a marked effect on the behavior of the structure and may, in fact, be responsible for failures unless they are properly provided for in the design.

This paper summarizes the results of a number of tests made at the University of Illinois in recent years to demonstrate the effect of details on the fatigue behavior of welded flexural members. Details such as splices, stiffeners, cover plates and attachments, all of which can be expected to produce reductions in the fatigue strength of the basic member, have been included. In addition, the fatigue behavior of these members is related to that of the basic material, thereby making it possible to obtain an indication of the effective stress concentration of the various details studied.

In this evaluation of laboratory data, the test conditions are related to actual service conditions; however, because of the many different combinations of loading obtainable in the field, only selected service conditions will be related directly to the data. Nevertheless, interpolations and extrapolations from the laboratory data provide a general indication of the behavior that can be expected under various service conditions. Though very limited in number, service records from actual structures in which fatigue failures have developed provide another means of relating the laboratory data with the field behavior.

DESCRIPTION OF MATERIALS AND TESTS

The tests, except for a few of those included in a preliminary series, were conducted on specimens fabricated from ASTM A373 steel. An ASTM A7 steel was used for the preliminary tests but did not differ greatly in chemical composition or in mechanical properties from the A373 steel used in the major portion of the program. The chemical composition and physical properties of the A373 steel are given in Table 1.

Manual arc welding with E7016 electrodes was used in the fabrication of most of the specimens for the tests discussed herein. The welds were deposited with reversed polarity, in the flat position, and with 5/32-in. electrodes for the assembly of the basic section and 1/8-in. electrodes for the attachment of stiffeners. All electrodes were stored in a drying oven to prevent absorption of moisture in the electrode coating.

The beams were tested in the 200,000-lb University of Illinois fatigue testing machine shown in Figures 1 and 2. These machines, when used for the testing of welded beams, are capable of applying a maximum midspan load of approximately 112,000 lb

TABLE 1

PROPERTIES OF ASTM A373[a] STEEL PLATES FOR WELDED BEAMS

Thickness (in.)	Chemical Content (%)						Physical Properties		
	C	Mn	P	S	Si	Cu	Yield Strength (psi)	Ultimate Strength (psi)	Elongation in 8-in. (%)
3/16[b]	0.23	0.60	0.023	0.030	0.050	0.065	42,040	65,490	28.3
1/2	0.23	0.56	0.018	0.024	0.070	0.020	35,990	64,780	31.0
3/4	0.18	0.94	0.007	0.019	0.050	0.025	38,700	63,400	29.0
1[b]	0.23	0.53	0.019	0.028	0.068	0.095	37,010	65,460	28.7

[a]ASTM A373 Structural Grade Steel for Welding. [b]Average for three heats of steel.

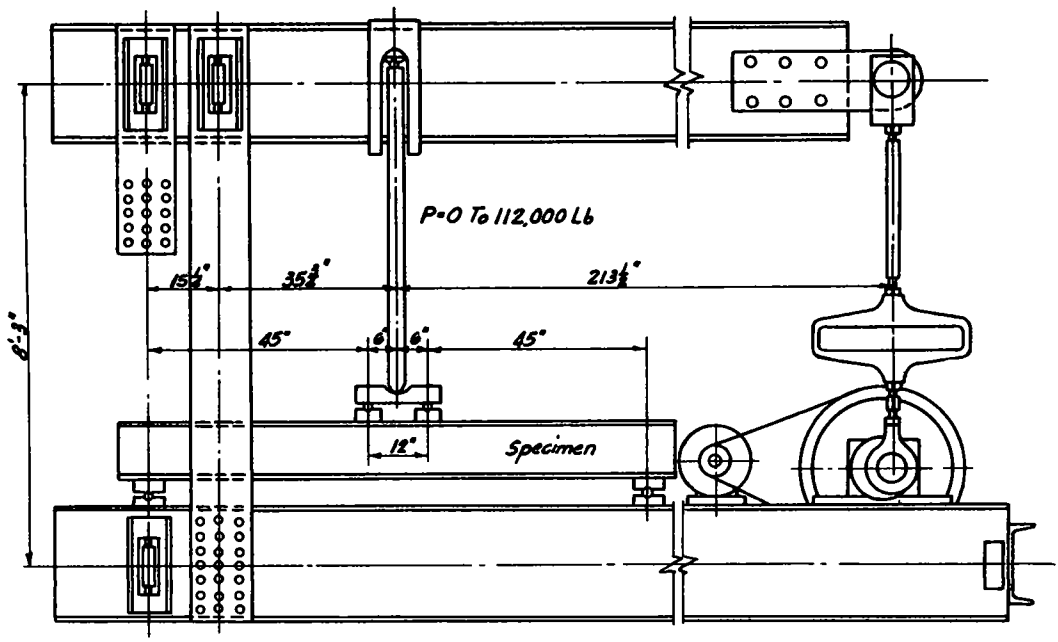

Figure 1. 200,000-lb Illinois fatigue testing machine adapted to test flexural specimens.

at a rate of 180 applications per min. Thus, approximately 250,000 cycles of loading can be applied in 1 day or 2,000,000 cycles of loading in approximately 8 days.

The capacity of the testing machines has limited to some extent the size of the members that can be tested. Nevertheless, they are large enough to permit the testing of beams with depths as great as 16 in. and spans of 8 ft 6 in. Although these members are relatively small in comparison with long-span welded bridges, they are of such a scale that the results of the tests will be directly applicable to the design of full-scale structures.

Most of the studies were conducted on a stress cycle in which the stress in the extreme fibres of the bottom flange of the member ranged from zero to tension. However, selected members have also been subjected to stress cycles of full reversal, or partial tension to a full tension in the extreme fibres. The use of these various cycles makes it possible to relate the behavior of the test members directly to the behavior that can be expected in bridges employing similar details.

The maximum values of test stress were selected to produce failures at lives rang-

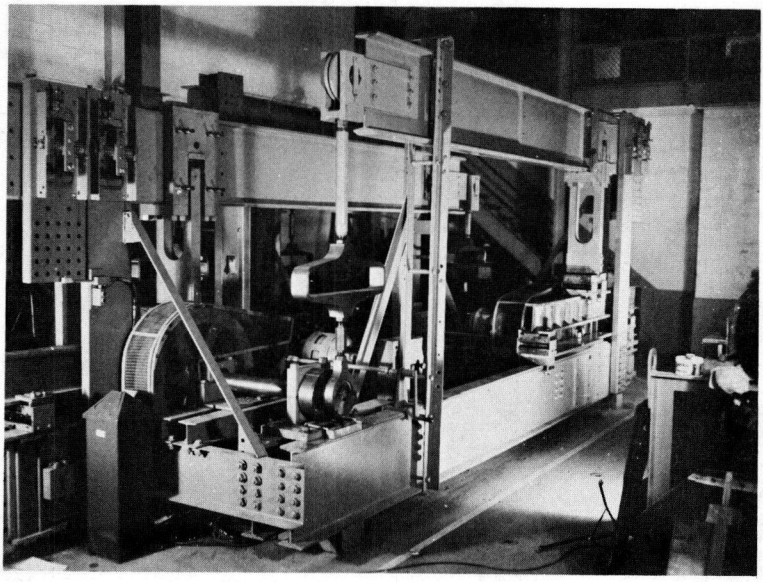

Figure 2. Flexural fatigue tests under way in 200,000-lb Illinois fatigue machines.

ranging from 100, 000 to 2, 000, 000 cycles and to provide S-N relationships which can be used to evaluate the effect of details upon the fatigue behavior of the test members. Such information also can be employed to develop design rules that will provide adequate resistance against fatigue.

After failure of the test members, the actual dimensions of the cross-section at the failures were measured and the stresses at these locations calculated using the general flexure formula,

$$s = \frac{Mc}{I}$$

Thus, although the applied loads were based on the nominal section of the test members, the failure stresses are based on the actual sections at which the failures occurred.

FATIGUE BEHAVIOR OF I-BEAMS

A limited number of tests have been conducted at the University of Illinois on plain rolled I-beams (2). Many more tests have been made on plain welded beams wherein a variety of sizes and shapes of members has been studied.

A summary of the fatigue strengths obtained for rolled beams of A7 steel, and welded beams of A7 and A373 steels are presented in Table 2. These results are only for members subjected to a stress cycle of zero to tension in the extreme fibres of the tension flange.

Comparing the fatigue resistance of the various beams with that of flat plates in the as-rolled condition, the fatigue resistance of the rolled beam appears only slightly different from that of the plain flat plate. However, the average fatigue strengths of the welded beams were about 5, 000 psi below those of the plain flat plates and those of the rolled beams. This decrease results from the details inherent in the fabricated beams—such details or factors as the weld and its geometry, the edge preparation of the various plates, the relative thickness of the components and the straightness of the member.

An examination of the test data indicates that for a stress cycle of 0 to 30, 000 psi, the fatigue life of the plain welded beams ranged from approximately 600, 000 to 2, 000, 000 cycles. This scatter, although relatively large in terms of life, is equivalent to a variation in fatigue strength of only about 7, 000 psi.

TABLE 2

FATIGUE STRENGTHS OF PLATES AND BEAMS
(Zero-to-Tension Cycle)

Type of Member	Type of Steel[a]	Fatigue Strength[b] (psi)	No. of Tests Averaged[c]
Plain plates	A7	31,700	---[d]
	A373	33,000	3
Rolled beams	A7	31,200	3
Welded beams	A7	28,200	4
	A373	26,500	16

[a]ASTM structural steels.
[b]N = 2,000,000.
[c]Extrapolation based on k = 0.135.
[d]Data from previous investigations.

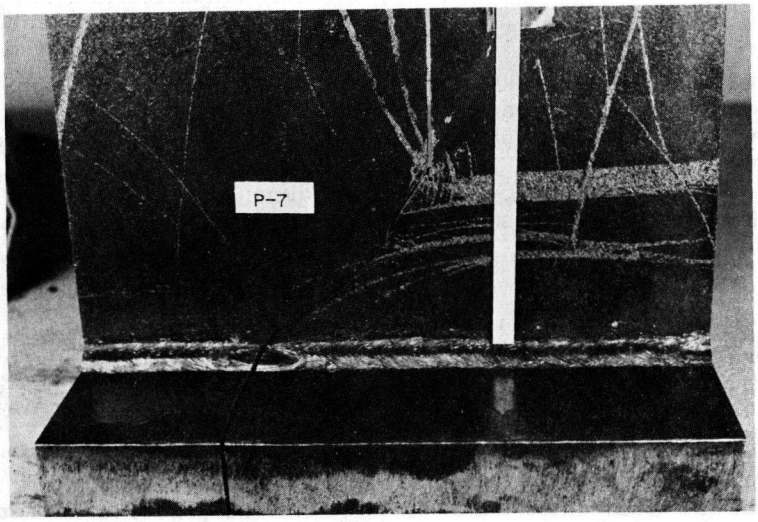

Figure 3. Fatigue crack initiating at weld crater.

One factor found to have an effect on the fatigue resistance of the welded beams is the ratio of the thickness of the flange to that of the web. In one series of tests on ASTM A7 steel beams the ratio was varied from 1.0 to 5.3. Although limited in number the tests, all conducted on the same stress cycle, gave lives ranging from 830,000 to 2,164,300 cycles. With so few tests, one would normally hesitate to draw conclusions concerning a factor such as the effect of the flange-to-web thickness ratio. However, the trend was consistent in all of the tests—the members with a thin web and heavy flanges had the greatest fatigue resistance when used in a plain welded beam.

In addition to the variation in fatigue life with the flange-to-web thickness ratio, a difference in the mode of failure was observed. The point of failure initiation was generally the same—in a weld crater of the fillet welds at the web-flange junction. However, the sequence of crack propagation differed somewhat for the various flange-to-web thickness ratios. For members with a low ratio (1 to 1), the cracks generally propagated through the flanges first and then into the web. For specimens with a high

flange-to-web thickness ratio (1 to 5.3), the initial direction of propagation was into the web. In the latter case, the rate of crack propagation decreased as the crack propagated toward the neutral axis and only when the crack in the web was 2 to 3 in. long did it begin to spread into the flange. This difference in crack propagation helps to explain, at least in part, the variation in fatigue life obtained from the specimens with various ratios of flange-to-web thickness.

Most of the plain-welded beams failed in the pure moment region of the members. The cracks generally initiated at a weld crater in the web-flange junction and propagated in a direction normal to the axis of the beams. However, one of the failures initiated at a weld crater a short distance outside the pure moment area and propagated through the flange and diagonally upward into the web. This change in direction of the fatigue crack was a result of the combined state of stress existing in the web; this fracture is shown in Figure 3. The photograph also shows the manner in which the fatigue cracks initiated in the weld craters. In the other members of this type, the cracks in the web propagated vertically. However, though the weld craters may provide the points at which the failures initiate, their effect on the fatigue strength of the members is not great (see Table 2).

EFFECT OF SPLICES ON FATIGUE BEHAVIOR

Splices are often used in welded girder bridges, particularly in those that are continuous structures. The details of such splices may be of several types; they may have the welds all in a single plane or staggered, and may be fabricated with or without cope holes at the flange splices. In addition, shop splices may be made in either the web or the flange alone. All of these details, because of their inherent stress concentrations, can be expected to have an effect on the fatigue resistance of the members.

Laboratory data are available from tests on splices and splice details of the types shown in Figure 4. A comparison of the test results for the various splices on a zero-to-tension stress cycle is presented in Figure 5. On examination, the slopes of the S-N curves appear different for the two basic types of splices; the curves are steeper for the members with the splice in a single plane than for those that are staggered. Also, the cope holes reduced the fatigue strength in both instances by approximately 2,000 to 3,000 psi. Thus, both the splice and the details of the splice affect the fatigue behavior of the members.

Good quality splices in thin-web members of the type shown in Figure 4, can usually be produced without cope holes, but with a thick web it may be necessary to use the cope holes to obtain a sound flange weld. Consequently, care must be exercised in extrapolating from the laboratory tests to actual service conditions; the details that prove best in the laboratory may not always be as effective in the field but may still be necessary.

A summary of the fatigue strengths of the various types of spliced members is presented in Table 3. The fatigue strength of the spliced beams can be made to approach or equal that of a plain plate with a transverse butt weld; however, the fatigue strength of the spliced members at 2,000,000 cycles is only about two-thirds as great as the fatigue strength of the plain plate material. Even the flange splice alone or the cope holes alone (specimen types C and F) have an effect on the fatigue strength of the members and again demonstrate the effect of welding and geometrical details on the fatigue behavior of the members.

Although most of the tests of spliced members were conducted on a stress cycle of zero to tension, cycles of full reversal and half-tension to full tension have been used for the type A and D splices. The results of these latter tests, showing the effect of stress cycle, are given in Figure 6. Again it is evident that the type D splice without cope holes had a slightly higher fatigue strength than did the splice fabricated with cope holes.

As the next step of this evaluation the fatigue data may be analyzed with respect to the current specifications of the American Welding Society for the design of welded highway and railway bridges (1). The results of such a comparison are given in Figure 7. The lines identified as AWS-15 and AWS-7 represent the AWS design relationships for butt welds subjected to tension.

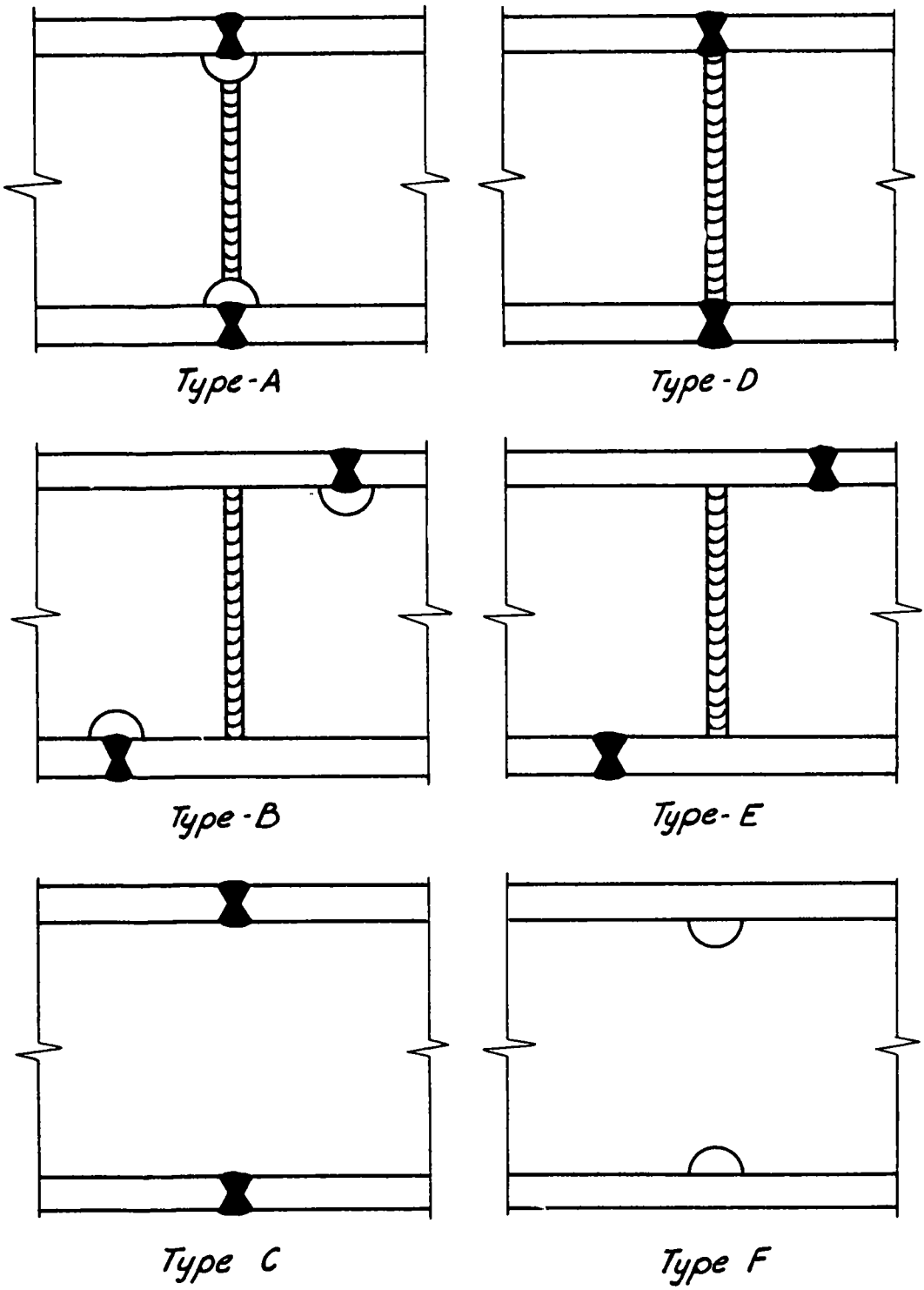

Figure 4. Details for splices in welded beams.

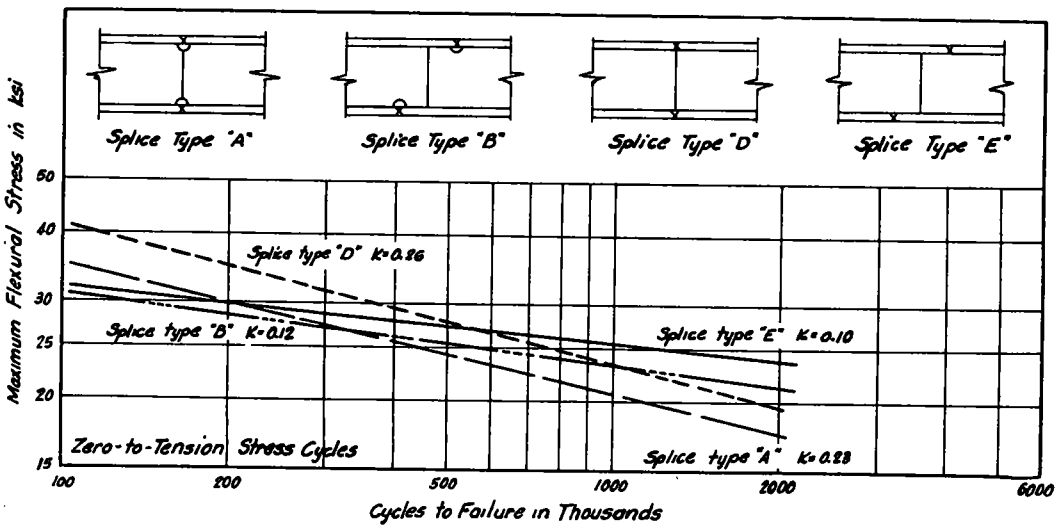

Figure 5. Comparison of test results for spliced beams.

TABLE 3

SUMMARY OF FATIGUE STRENGTHS FOR SPLICED MEMBERS
(Zero-to-Tension Cycle)

Type of Member[a]	Fatigue Strength (psi)	
	n = 100, 000	n = 2, 000, 000
Plain plate	-	33, 000
Transverse butt welded joint (as welded)	-	22, 500
In-line splice with cope holes, type A (Fig. 4)	33, 500	17, 500
Staggered splice with cope holes, type B (Fig. 4)	31, 000	21, 000
In-line splice, as welded, type D (Fig. 4)	40, 000	19, 500
Staggered splice, as welded, type E (Fig. 4)	32, 000	23, 000
Flange splice only, as welded, type C (Fig. 4)	-	26, 000(2)[b]
Cope hole only, type F (Fig. 4)	-	23, 000(3)[b]

[a]Fabricated from ASTM A373 steel.
[b]Number in parentheses indicates number of tests averaged when extrapolation based on only a small number of tests.

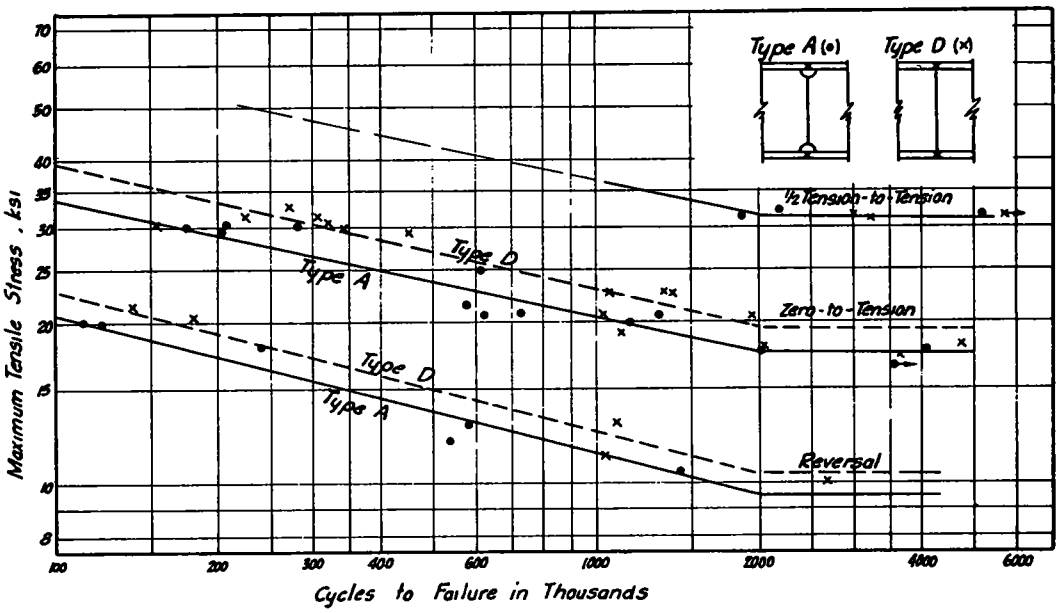

Figure 6. Results of fatigue tests on welded beams with splices.

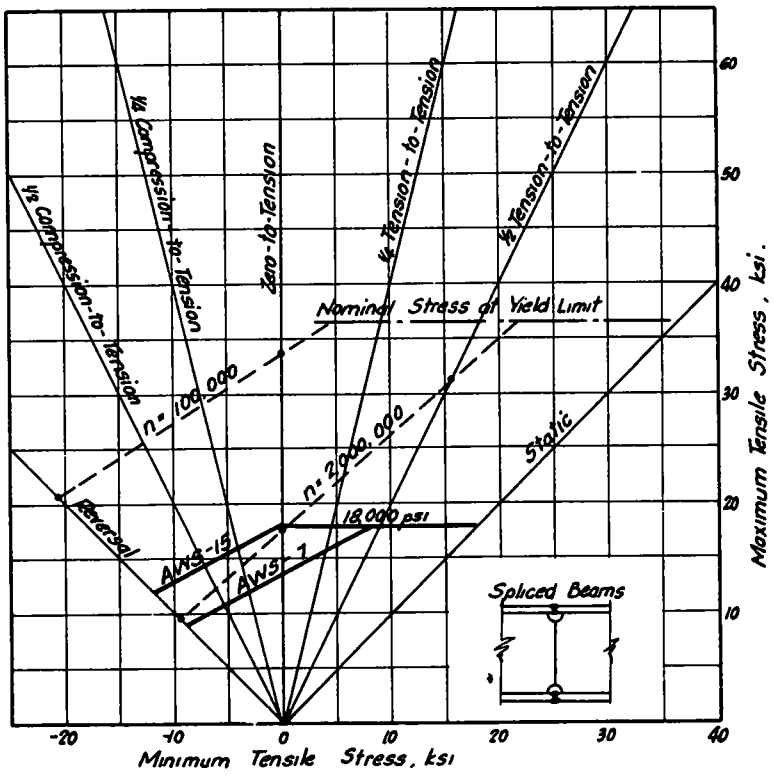

Figure 7. Relationship between test results for spliced beams and design specifications.

AWS Formula 7 (butt weld at 2, 000, 000 cycles):

$$A = \frac{\text{Max.} - 1/2\ \text{Min.}}{13,500} \text{ or } s = \frac{13,500}{1 - 1/2\,k}$$

$$\text{but} \geq \frac{\text{Max.}}{18,000} \qquad \text{but} \leq 18,000$$

$$\text{where } k = \left(\frac{\text{Min.}}{\text{Max.}}\right)$$

AWS Formula 15 (butt weld at 100, 000 cycles):

$$A = \frac{\text{Max.} - 1/2\ \text{Min.}}{18,000} \text{ or } s = \frac{18,000}{1 - 1/2\,k}$$

$$\text{but} \geq 18,000 \qquad \text{but} \leq 18,000$$

$$\text{where } k = \left(\frac{\text{Min.}}{\text{Max.}}\right)$$

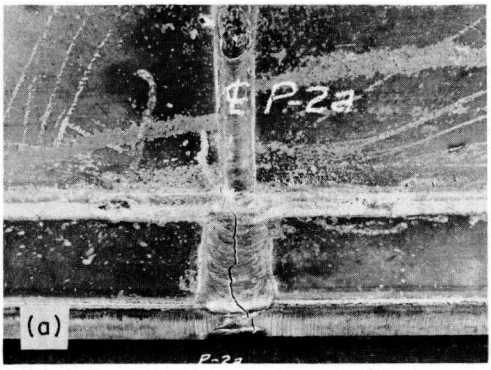

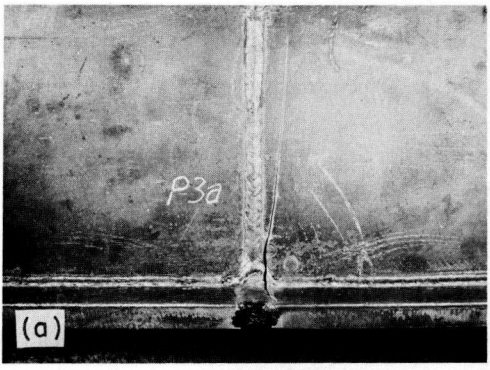

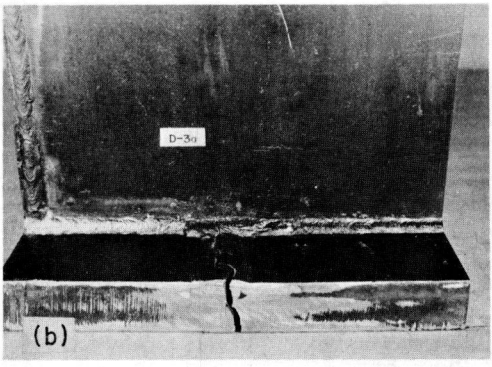

Figure 8. Flange-weld fatigue cracks in beams with butt-welded splices: (a) in-line-splice, and (b) staggered splice.

Figure 9. Fatigue cracks at edge of flange welds in beams with butt-welded splices: (a) in-line splice, and (b) staggered splice.

Line AWS-15 is generally thought to represent a condition comparable to 100, 000 cycles of loading, whereas line AWS-7 corresponds to a condition representing 2, 000, 000 cycles of loading. In the diagram it is evident that when the stress cycle varies from one of partial tension to full tension, the design factor of safety (relationship of fatigue strength to allowable design stress) may become relatively large. However, under a cycle of full reversal, a spliced member that is expected to receive 2, 000, 000 cycles of maximum loading during its lifetime will have a relatively small factor of safety.

A further indication of the fatigue behavior of the spliced members can be obtained from an examination of the fractures of these members. Although the number of tests was not great, a variety of failures was obtained. Some failures occurred in the weld (Fig. 8), some initiated at the toe of the butt weld (Fig. 9), and others initiated at the toe of the fillet welds associated with the cope holes (Fig. 10). In spite of this variety of failures the fatigue resistance of the various members did not differ greatly.

EFFECT OF STIFFENERS ON FATIGUE BEHAVIOR

The American Welding Society's specification for welded highway and railway bridges (1) states:

> Ends of stiffeners and other attachments may be welded to flanges only at points where the flanges carry compressive stress or where the tensile stress does not exceed 75 percent of the maximum allowable stress permitted by the applicable general specification.

Thus, the specifications are concerned only with the effect the stiffeners have on the behavior of the flanges and not with their effect on the behavior of the web. Nevertheless, the results of recent tests suggest that both the flanges and webs may need to be considered in designing for fatigue.

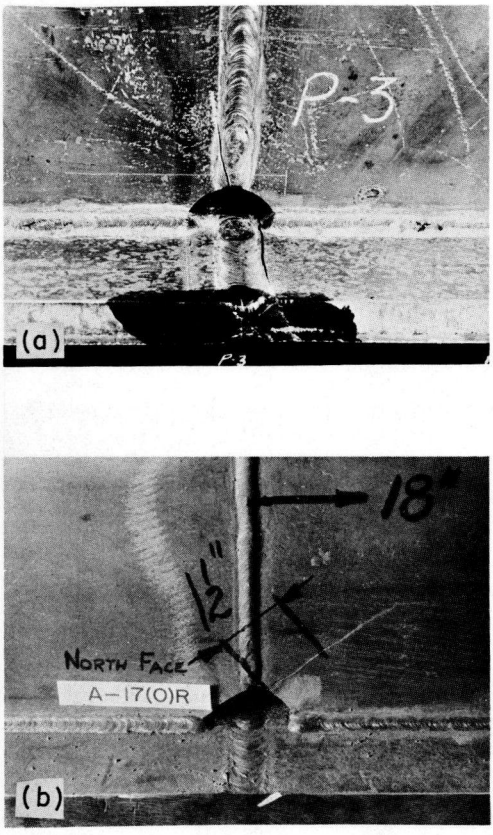

Figure 10. Fatigue cracks at cope-holes: (a) flange failure at toe of fillet, and (b) failure in web at cope hole.

In tests recently conducted at the University of Illinois, the effects of various stiffeners on the fatigue behavior of welded flexural members have been studied. Figure 11 shows the variations in the details studied, including members with stiffeners on one or both sides of the web, members with and without the stiffener attached to the tension and compression flanges, members with the stiffeners attached to the web with intermittent fillet welds, and members with stiffeners attached only over a part of the web. Although these are but a few of the many details that could be used, they provide a general picture of the effect of stiffeners on the flexural behavior of the members.

All fatigue tests conducted on beams with stiffeners were made with a stress cycle of zero to tension in the extreme fibres of the bottom flange. The results of these tests, for five types of stiffeners, are shown by the S-N diagram in Figure 12. It should be noted, however, that these data are presented on the basis of the maximum flexural stress in the extreme fibres of the test member and not

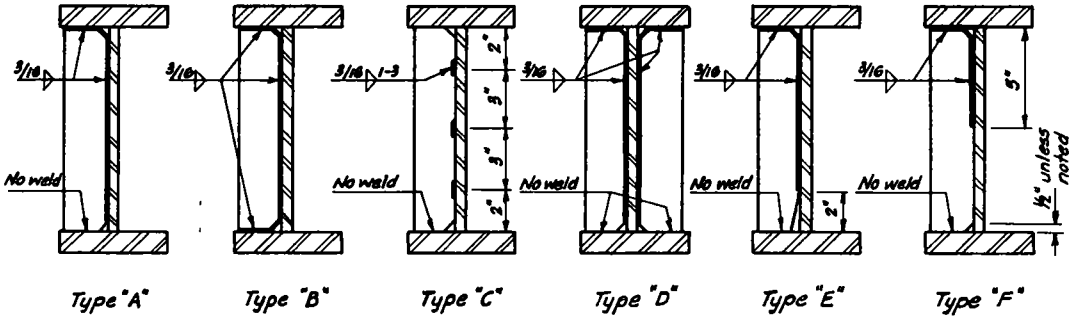

Figure 11. Details of various stiffener types.

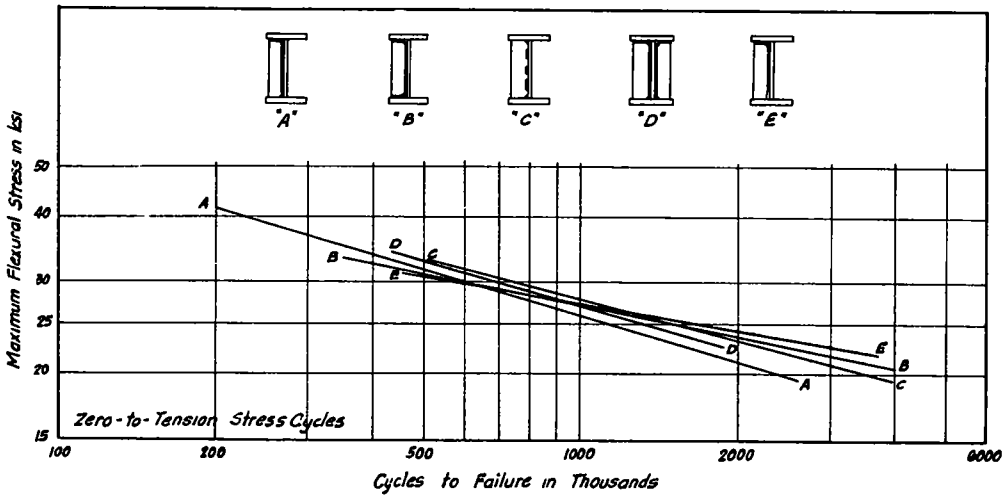

Figure 12. S-N diagram for stiffened beams based on maximum flexural stress.

necessarily on the basis of the stress at the point of failure. Nevertheless, excellent consistency was obtained for all of the stiffener details included in the study. Obviously the members all have about the same total flexural resistance; however, because the failures occurred at various points along the length of the span, the members did not necessarily have the same flexural fatigue strength at the points of failure.

In evaluating the data from the stiffener tests, several factors must be considered. The most important of these are the failure location and the general occurrence of fractures at stiffeners that were not in the region of pure moment. In fact, most of the fractures occurred at stiffeners located where the flexural stresses were considerably lower than the maximum flexural stresses. After a thorough examination of the data, the best correlation was obtained when the data were analyzed on the basis of the maximum principal tensile stress (including the effect of the shear) at the point of failure. The following relationships were used to determine the maximum principal tensile stress at the point where failure initiated.

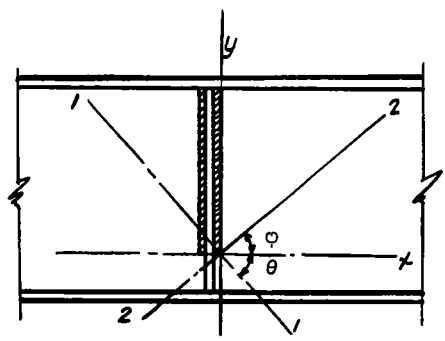

$$\sigma_p = \frac{\sigma_x + \sigma_y}{2} \pm \sqrt{\left(\frac{\sigma_x - \sigma_y}{2}\right)^2 + \tau^2} \quad (1)$$

$$\tau_p = \frac{\sigma_1 - \sigma_2}{2} = \sqrt{\left(\frac{\sigma_x - \sigma_y}{2}\right)^2 + \tau^2} \quad (2)$$

$$\tan 2\theta = -\frac{2\tau}{\sigma_x - \sigma_y} \quad (3)$$

$$\varphi = 90^\circ - \theta \quad (4)$$

where

$$\tau = \frac{VQ}{It}, \quad \sigma_y = 0, \quad \sigma_x = \frac{My}{I}$$

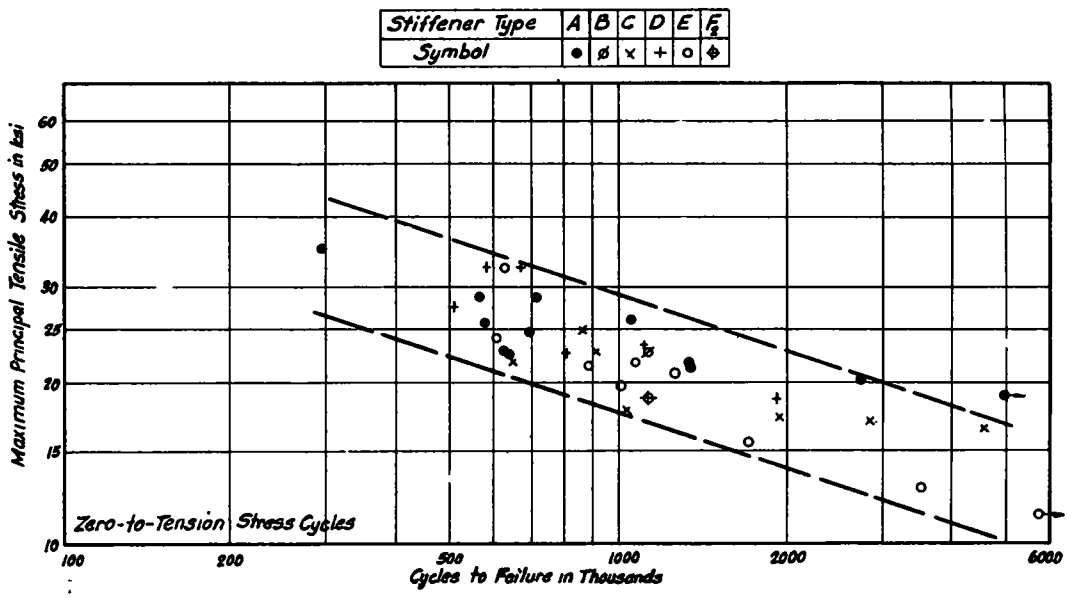

Figure 13. S-N diagram for maximum principal tensile stress at failure section.

The comparison obtained on the basis of a principal stress analysis is shown in Figure 13. Although there is still a scatter in the test results, the band is well defined for the entire range of lives and stresses used in tests.

A further indication of the fatigue behavior of the members with stiffeners can be obtained from an examination of the fatigue failures. As might be expected, a variety of failures was obtained. Members with types A, D, or E stiffeners and members with continuous welds connecting the stiffeners to the web had failures that initiated at the bottom of the fillet welds connecting the stiffeners to the web. Upon initiation, these cracks propagated diagonally upward into the web in a direction approximately normal to the principal tensile stress.

Another indication of the importance of the principal stress is the fact that the fractures were just as likely to initiate at a section near the supports as they were to initiate near the center of the beam.

Figure 14 shows a typical failure at a stiffener. In this instance, the crack initiated in the web at a point 25 ½ in. from the beam support and propagated at an angle of approximately 50 deg. The computed angle for the maximum principal stress at this location was only slightly greater than 50 deg. The maximum flexural stress in this same member occurred at approximately 45 in. from the supports.

The fatigue cracks in members with type C stiffeners initiated at either the the top or bottom of the intermittent fillet welds connecting the stiffeners to the web. These cracks were then found to propagate diagonally upward into the web and downward to the flange. An indication of one such failure is shown in Figure 15. This failure initiated in the web of the member at a distance of approximately 20 in. from the support.

The members with type B stiffeners were the only ones for which the stiffeners were welded to the tension flange. These members generally failed at the toe of the fillet weld connecting the stiffener to the flange of the beam, in the region near the maximum moment, and propagated vertically through the flange and up into the web. Nevertheless, the total fatigue resistance of the members with the type B stiffeners (those welded all around) was as great or greater than that of the members fabricated with the other stiffener details.

Figure 14. Web crack at type A stiffener (continuous web weld).

Figure 15. Web crack at type C stiffener (intermittent web weld).

In view of the fatigue behavior that has been observed, it may be desirable to re-examine the restrictions of current specifications for the attachment of stiffeners. It would appear that when stiffeners are not welded to the tension flange of a flexural member that is subjected to repeated loads, the shear in the web of the member should be considered. This consideration need not include the effect of shear as a separate factor but only as it affects the principal tensile stress in the web of the member.

EFFECT OF COVER PLATES ON FATIGUE BEHAVIOR

Because attachments to the tension flange of a beam change its geometry and produce stress concentrations, it can be expected that such attachments will also change the fatigue behavior of the member at the sections where such attachments are affixed. A partial-length cover plate on a beam, for example, can be expected to have a marked effect on the fatigue behavior of the beam.

Recently, studies were made at the University of Illinois on a variety of cover and flange plate details. The end details used for the cover plates are shown in Figure 16 and flange transitions in Figure 17. Varying the width or thickness of the flange plate in the manner shown in Figure 17 provides a more uniform transfer of stress than does the cover plate and can be expected to have a greater fatigue resistance than that of the member with a partial-length cover plate. However, the partial-length cover plate is a simple, economical, and effective means of providing an increase in section modulus.

Only a limited number of tests have been conducted on members with various cover plate details. Nevertheless, the data from these tests have been sufficient to provide S-N curves for each of the details and a loading cycle of zero to tension. A summary of these data (Table 4) shows that there is a relatively large variation in the fatigue resistance of the members with various cover plate or flange plate details. At 2,000,000 cycles the fatigue strengths were found to range from 11,300 to 14,500 psi for partial-length cover plates. However, the flange transitions provided a fatigue strength of approximately 19,000 psi.

A study of Table 4 indicates that any means used to make the change in cross-section more gradual is effective in increasing the fatigue strength of the beam under repeated loads. At the higher loads, the beams that exhibited the best behavior were those with the type F cover plate; this type of end detail combined the beneficial effects of tapering the end of the cover plate and of eliminating trans-

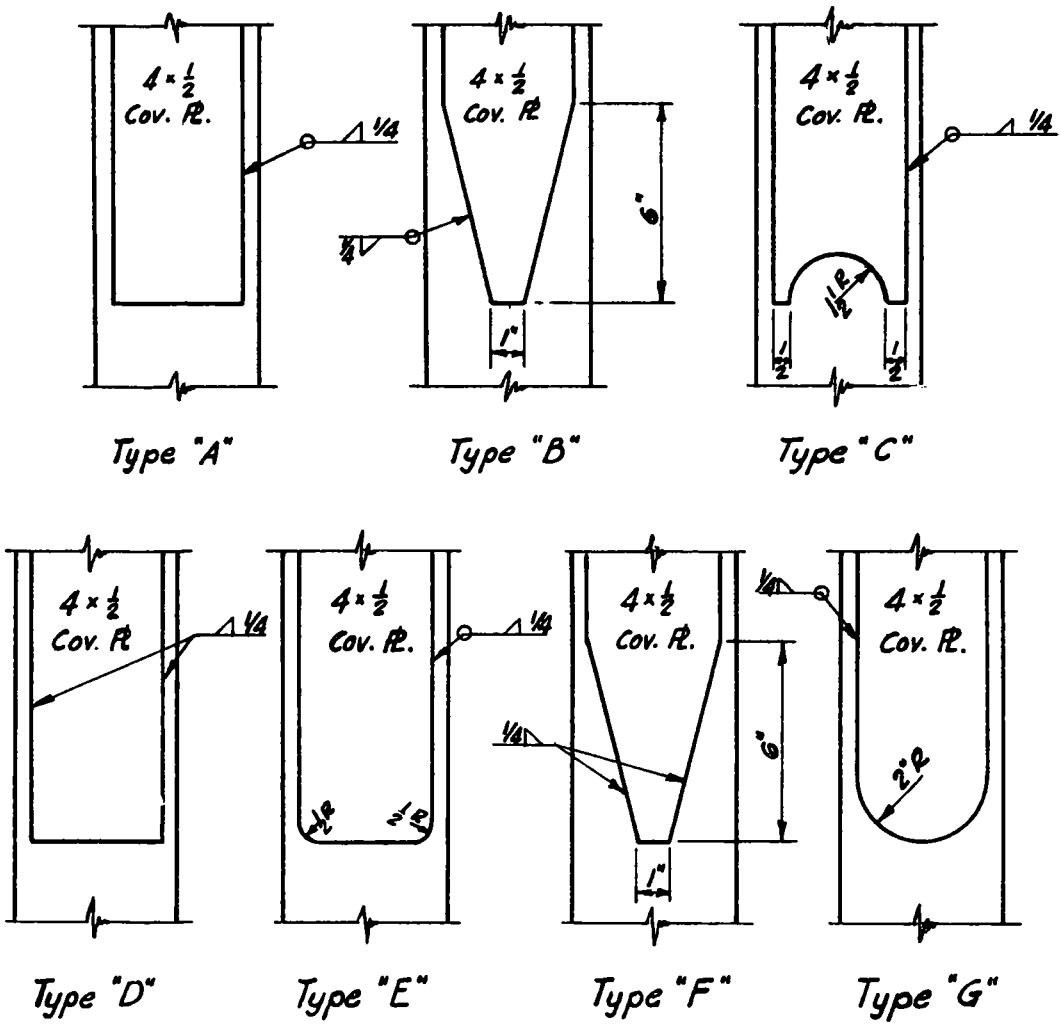

Figure 16. Details of various types of cover plates.

TABLE 4

SUMMARY OF FATIGUE STRENGTHS OF BEAMS WITH VARIOUS CHANGES IN FLANGE AREA
(Zero-to-Tension Cycle)

Description	$F_{100,000}$ psi	$F_{2,000,000}$ psi
Partial-length cover plates, square ends with continuous weld all around (Type A)	26,500	11,300
Partial-length cover plates, tapered ends with continuous weld all around (Type B)	34,000	11,400
Partial-length cover plates, concave profile with continuous weld all around (Type C)	30,700	14,500
Partial-length cover plates, square ends with continuous welds along edges only (Type D)	34,700	12,100
Partial-length cover plates, tapered ends with continuous weld along edges only (Type F)	37,800	13,400
Partial-length cover plates, convex profile with continuous weld all around (Type G)	29,400	11,600
Butt-welded flange transition, tapered in width (Type J)	34,900	19,500
Butt-welded flange transition, tapered in thickness (Type K)	34,600	18,500

verse welds. At the lower loads (longer life), beams with the type C end detail gave the best results. However, the difference in fatigue behavior of members with these various details was not great.

The omission of the transverse welds at the ends of the cover plates appears to provide an increase in the fatigue resistance of the members. Nevertheless, the most effective means of increasing the fatigue resistance of the beams of variable section was to vary the flange in width or thickness, in the manner shown in Figure 17. In this way, a fatigue resistance almost as great as that of a spliced beam was obtained, again demonstrating the advantage of reducing the stress concentration to a minimum when fatigue is involved.

RELATIONSHIP BETWEEN FATIGUE BEHAVIOR AND DESIGN SPECIFICATIONS

A variety of welded details and their effect on the fatigue behavior of a welded beam have been discussed. Although the test data considered herein provide a general indication of the fatigue behavior of welded beams and girders, it is evident

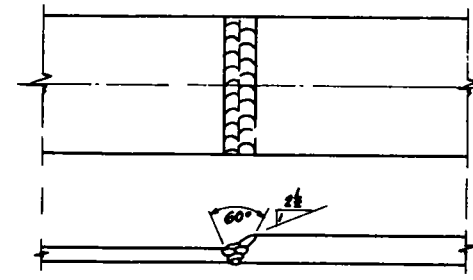

(a) Transition in Flange Thickness (Type K)

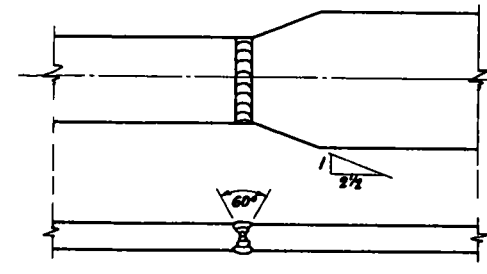

(b) Transition in Flange Width (Type J)

Figure 17. Weld details for flanges of beams with flange-plate transitions.

that the results in individual S-N diagrams or from a single series of tests can not provide sufficient information to relate directly the behavior of the members of all field or service conditions. However, effective extrapolations can be made to service conditions.

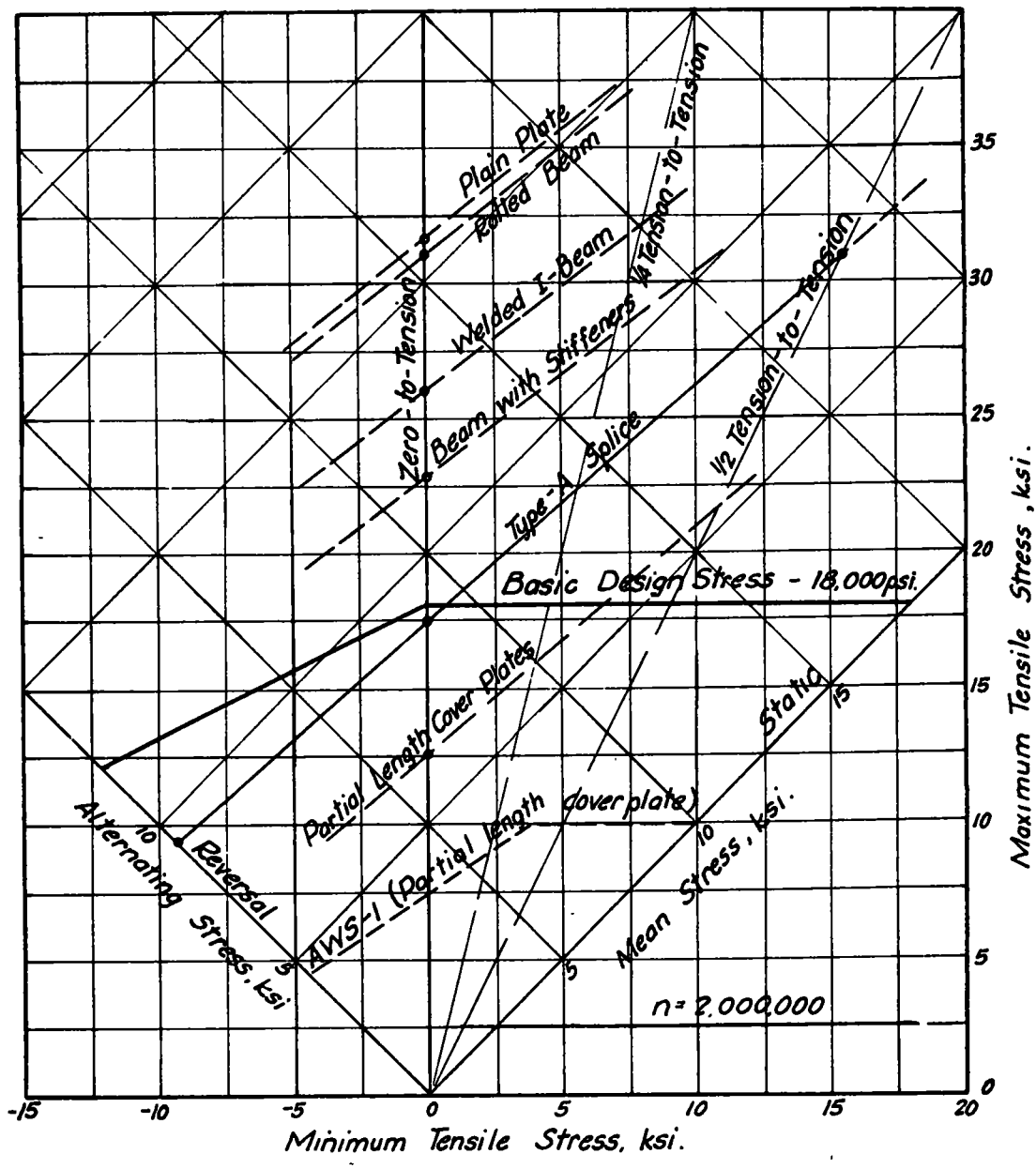

Figure 18. Relationship between fatigue strength of welded beams with basic design stresses.

All of the weld details are known to reduce the fatigue resistance of a welded beam or girder below that of the basic material. However, the degree of this reduction depends on the magnitude of the stress concentrations resulting from the details. A summary of the approximate fatigue strengths of welded beams with various details is presented in Table 5. Here it may be seen that most of the details, although decreasing the fatigue strength of the basic material, provide members with a relatively high fatigue resistance; only the partial-length cover plate produces a major reduction in the fatigue strength of the material.

The data of Table 5 provide an indication only of the fatigue strength of the members at 2,000,000 cycles and for a zero-to-tension loading cycle. To understand more fully the general fatigue behavior of the members, it is necessary to consider what might be expected under other loading conditions. Data are not available to describe directly the behavior of the members under various loading conditions but, by means of relationships such as shown in Figure 18, it is possible to relate approximately the behavior of welded flexural members to the maximum stresses employed in design.

In Figure 18, the basic tensile design stresses for bridges are compared with the results of the fatigue tests discussed herein. The data demonstrate that plain welded beams and those with stiffeners should not fail in fatigue under any conditions of loading, so long as the basic design stresses are not exceeded. However, when splices or partial-length cover plates are used, further reductions in design stress may be necessary for members subjected to repeated loads; the magnitude of the reduction depending on the expected life and the loading conditions.

TABLE 5

SUMMARY OF APPROXIMATE FATIGUE STRENGTHS OF WELDED BEAMS WITH VARIOUS DETAILS
(Zero-to-Tension Cycle)

Member or Section	$F_{2,000,000}$ psi	Ratio to Plain Plate
Plain plate	31,700	1.0
Rolled I-beam	31,200	0.98
Welded I-beam	26,500	0.83
Welded beam with stiffeners	23,000	0.73
Welded beam with splice	20,000	0.63
Welded beam with butt-welded flange transitions	19,000	0.60
Welded beam with partial-length cover plate	12,500	0.39

In general, welded girder highway bridges are subjected to loads that produce cycles of maximum stress ranging from $\frac{1}{4}$ or $\frac{1}{2}$ tension to tension. Under such loading conditions, all but members with partial-length cover plates and possibly members with splices would appear to have adequate fatigue capacity at the basic design stresses for 2,000,000 cycles of loading. However, the magnitude of the factor of safety for the various types of members varies considerably. In the case of members with partial-length cover plates or those with splices, lower design stresses are necessary to provide a suitable factor of safety.

The current provisions of the AWS specifications for welded highway and railway bridges provide the following reduced allowable unit stresses for members with partial-length cover plates and subjected to 2,000,000 cycles or more of loading.
AWS Formula 1 (tension in member adjacent to fillet welds):

$$A = \frac{\text{Max.} - 2/3\ \text{Min.}}{7,500} \quad \text{or} \quad s = \frac{7,500}{1 - 2/3\ k}$$

$$\text{but} \geq \frac{\text{Max.}}{10,000} \qquad \text{but} \leq 10,000$$

$$\text{where } k = \left(\frac{\text{Min.}}{\text{Max.}}\right)$$

This relationship, shown in Figure 18 as AWS-1, provides safety against failure in members with partial-length cover plates for all types of stress cycles. The relationships shown in Figure 7 provide for members with splices.

On the basis of the data discussed herein it can be seen that when the current specifications are correctly applied, welded beams and girders of highway bridges, if properly fabricated, should have adequate fatigue capacity. However, in view of the web failures observed in the laboratory tests, further consideration should be given to the effect of shear (principal tensile stresses in the webs) on the fatigue behavior of members with thin webs.

ACKNOWLEDGMENTS

The fatigue tests described herein were conducted in the structural laboratories of the Civil Engineering Department at the University of Illinois under the sponsorship of the Bureau of Public Roads, Department of Commerce. The tests were conducted by B. J. Goodall, W. E. Fisher, N. G. Kouba and L. R. Hall, research assistants in Civil Engineering at the University of Illinois.

The Fatigue Committee of the Welding Research Council acted in an advisory capacity in the planning of the program. However, the views expressed are those of the authors and do not necessarily reflect the views of the sponsor or the Fatigue Committee.

REFERENCES

1. "Standard Specifications for Welded Highway and Railway Bridges." American Welding Society (1956).
2. Wilson, W. M., "Flexural Fatigue Strength of Steel Beams." Univ. of Ill. Engineering Experiment Station, Bull. 377 (1948).
3. Wilson, W. M., and Munse, W. H., "The Fatigue Strength of Various Details Used for the Repair of Bridge Members." Univ. of Ill. Engineering Experiment Station, Bull. 382 (1949).
4. Wilson, W. M., Munse, W. H., and Snyder, I. S., "Fatigue Strength of Various Types of Butt Welds Connecting Steel Plates." Univ. of Ill. Engineering Experiment Station, Bull. 384 (1950)
5. Stallmeyer, J. E., Munse, W. H., and Goodal, B. J., "Behavior of Welded Built-Up Beams Under Repeated Loads." Welding Jour. 36: No. 1 (Jan. 1957).
6. Conyers, A. L., and Ozell, A. M., "Transfer of Stresses in Welded Cover Plates." Department of Civil Engineering, Univ. of Florida, Preliminary Report (Feb. 1959)
7. Hall, L. R., and Stallmeyer, J. E., "The Fatigue Strength of Flexural Members." Department of Civil Engineering, Univ. of Ill., Preliminary Report (April 1959)
8. Fisher, W. E., and Stallmeyer, J. E., "Behavior of Welded Built-Up Beams Under Repeated Loads." Department of Civil Engineering, Univ. of Ill., Preliminary Report (March 1958).
9. Kouba, N. G., and Stallmeyer, J. E., "The Behavior of Stiffener Beams Under Repeated Loads." Department of Civil Engineering, Univ. of Ill., Preliminary Report (April 1959).

THE NATIONAL ACADEMY OF SCIENCES—NATIONAL RESEARCH COUNCIL is a private, nonprofit organization of scientists, dedicated to the furtherance of science and to its use for the general welfare. The ACADEMY itself was established in 1863 under a congressional charter signed by President Lincoln. Empowered to provide for all activities appropriate to academies of science, it was also required by its charter to act as an adviser to the federal government in scientific matters. This provision accounts for the close ties that have always existed between the ACADEMY and the government, although the ACADEMY is not a governmental agency.

The NATIONAL RESEARCH COUNCIL was established by the ACADEMY in 1916, at the request of President Wilson, to enable scientists generally to associate their efforts with those of the limited membership of the ACADEMY in service to the nation, to society, and to science at home and abroad. Members of the NATIONAL RESEARCH COUNCIL receive their appointments from the president of the ACADEMY. They include representatives nominated by the major scientific and technical societies, representatives of the federal government, and a number of members at large. In addition, several thousand scientists and engineers take part in the activities of the research council through membership on its various boards and committees.

Receiving funds from both public and private sources, by contribution, grant, or contract, the ACADEMY and its RESEARCH COUNCIL thus work to stimulate research and its applications, to survey the broad possibilities of science, to promote effective utilization of the scientific and technical resources of the country, to serve the government, and to further the general interests of science.

The HIGHWAY RESEARCH BOARD was organized November 11, 1920, as an agency of the Division of Engineering and Industrial Research, one of the eight functional divisions of the NATIONAL RESEARCH COUNCIL. The BOARD is a cooperative organization of the highway technologists of America operating under the auspices of the ACADEMY–COUNCIL and with the support of the several highway departments, the Bureau of Public Roads, and many other organizations interested in the development of highway transportation. The purposes of the BOARD are to encourage research and to provide a national clearinghouse and correlation service for research activities and information on highway administration and technology.